

## Heat and mass transfer analysis of passive solar still with nanoparticles, operating at different water depth and various slope of glass cover

Vikas Kumar Thakur\*, Manoj Kumar Gaur

Madhav Institute of Technology and Science, Department of Mechanical Engineering, Gwalior 474005, M.P., India, emails: vikasthakur1502@gmail.com (V.K. Thakur), gmanojkumar@rediffmail.com (M.K. Gaur)

Received 28 March 2021; Accepted 18 July 2021

---

### ABSTRACT

The paper presents the effect of water depth and tilt angle on the productivity of solar still operating with CuO and ZnO nanoparticles. Three solar stills at tilt angle of 11°, 26° and 41° are fabricated and tested for their performance at three water depth (4, 5 and 10 cm) and CuO and ZnO nanoparticles. The solar stills are operated in winter season and their basin area is 1 m<sup>2</sup>. The effect of water depth, tilt angle and type of nanoparticles on convective and evaporative heat transfer coefficient is also studied. The productivity is found higher at low water depth (4 cm) and at higher tilt angle (41°). The productivity of solar still with CuO nanoparticles is 2.03 L/m<sup>2</sup>d. While for convective solar still and solar still with ZnO nanoparticles, it is 1.43 and 1.54 L/m<sup>2</sup>d respectively. The calculated internal heat transfer coefficient of solar still with CuO nanoparticles is 155.2% higher reported than convective solar still while with ZnO nanoparticles, it is 64.8% higher than conventional solar still. It is observed that productivity of solar still with nanoparticles for 11° tilt angle is even higher than that of recommended angle of solar still for winter season (41° for winter climatic condition).

*Keywords:* Nanoparticles; Tilt angle; Distilled water; Water depth; Heat and mass transfer; Solar still

---

### 1. Introduction

Solar still (SS) is a sustainable and simple device that provides pure water without polluting the atmosphere. Due to its low production rate it is not popular in the market. Researchers are constantly trying to increase the productivity of SSs using various techniques. Many of the researchers have done theoretical and experimental study on passive and active SSs and they found that passive SS is more sustainable in terms of pure water productivity as compared to active SS.

Numerous experimental and theoretical studies were conducted by many researchers [1–6] to improve the performance of SS like: SS with rotating discs are used with wick material [7,8], single and double slope SS [9,10], and SS with external condenser [11]. It is observed that the productivity is strongly influenced by parameters like tilt angle

of glass cover, water depth, and heat absorbed/ transferred from basin [12,13], etc. In the present research, the effect of different nanoparticles, different water depth and different tilt angle on the internal heat transfer coefficient is studied.

### 2. Previous work on solar still with nanoparticles

Nanoparticles are used to increase thermal conductivity and thermal capacity of base fluid (water). This gives the higher yield as compared to conventional SS. Nanoparticles have been used by many authors to improve the daily yield of the traditional SS. Lot of research had been done on past using different nanoparticles and at different concentrations [14].

El Hadi Attia et al. [15], tested the performance of SS manufactures using steel, zinc and copper plate. Due to high thermal conductivity of copper, it is able to rapidly transmit

---

\* Corresponding author.

the absorbed solar radiation to the base fluid, hence water get heated quickly and starts evaporating in very less time as compared to zinc and steel plate SS. Essa et al. [16] improve the performance of stepped SS by using suspended trays, mixture of  $\text{Al}_2\text{O}_3$  nanoparticles and PCM (Paraffin wax), external condenser and a fan. Suspended tray increase the surface area of the brackish water, hence basin water gets converted into vapor rapidly. Nanoparticles having good thermal capacity stores more thermal energy in the PCM that maintains the higher basin temperature for a longer duration after sunshine hours.

Shanmugan and Essa [17] used copper sheet in the basin area of the single slope SS to increase its radiation absorption capacity. SS having Copper sheet coated with mixture of  $\text{TiO}_2$  and  $\text{Cr}_2\text{O}_3$  nanoparticles gives 7.89 L of fresh water in summer and 5.39 L in winter season. As in summer season, the solar intensity is higher as compared to winter season. Kabeel et al. [18] fabricated and tested the tubular SS using mixture of graphene oxide nanoparticles and PCM. Tubular SS with mixture of nanoparticles and PCM attained  $5.62 \text{ kg/m}^2$ , whereas still with only PCM and still without PCM achieved  $3.35$  and  $2.59 \text{ kg/m}^2$  distilled water in a day respectively. This is so because PCM with nanoparticles achieved 52% higher thermal conductivity as compared to PCM without nanoparticles.

To preheat the feed water before entering the basin a solar water heater with nanoparticles ( $\text{TiO}_2$ ,  $\text{Al}_2\text{O}_3$  and  $\text{ZnO}$ ) were used by Carranza et al. [19]. It was concluded that higher thermal conductive nanoparticles gives higher productivity. Condenser, solar water heater and  $\text{CuO}$  nanoparticles have been used by the Abdullah et al. [20] to enhanced the fresh water productivity of the rotating-drum SS. The modified rotating drum SS gives 350% higher productivity as compared to conventional SS. A tubular SS was developed by Arani et al. [21], in which the fins were provided in the absorber plate and it was painted with nanoparticles mixed black paint. It was observed that productivity rises by 55.28% as compared to conventional SS. Use of Fins increased the radiation absorption area and evaporation surface area, and nanoparticles mixed paint increased the radiation absorption capacity and heat transfer capacity of the absorber plate.

Panchal et al. [22] used the manganese oxide nanoparticles mixed black paint to paint the inner surface of single slope SS. It was found that with increase in concentration of the nanoparticles in black paint productivity also increases. The modified SS gives 19.5% higher productivity than the conventional SS.

Khanafer and Vafai [23] had developed a correlation on the basis of temperature, size, and concentration for the thermal conductivity of  $\text{CuO}$ ,  $\text{TiO}_2$  and  $\text{Al}_2\text{O}_3$ . Due to the metallurgical properties, optical properties, and plasmon resonance absorption bands nanoparticles absorbs the more amount of solar radiation. An experimental investigation was carried out by Chen et al. [24] to test the sunlight absorption characteristic of nanoparticles, in which silver nanoparticles were used in the base fluid to increase solar thermal conversion efficiency. Subhedar et al. [25] experimentally investigate the performance of conventional single slope SS, integrated with the parabolic trough collector for preheating the water.  $\text{Al}_2\text{O}_3$  nanoparticles had been

mixed in the basin water to enhance its thermal physical properties. It was found that the productivity of the still without nanoparticles was 1.1 L while with nanoparticles it was 1.747 L.

The effect of four different nanoparticles ( $\text{Al}_2\text{O}_3$ ,  $\text{ZnO}$ ,  $\text{Fe}_2\text{O}_3$  and  $\text{SnO}_2$ ) in the performance of single slope passive SSs was studied by Elango et al. [26], Graphite and copper oxide nanoparticles were added to the base fluid by Sharshir et al. [27] and Sahota et al. [28] also studied the effect on performance of SS by using  $\text{Al}_2\text{O}_3$ ,  $\text{TiO}_2$ , and  $\text{CuO}$ . It was found that nanoparticles with high thermal conductivity give higher productivity.

$\text{Al}_2\text{O}_3$  and  $\text{CuO}$  nanoparticles at three different concentrations (0.1%, 0.2% and 0.3%) were used in concrete based passive SS by Navale [29]. It was found that  $\text{CuO}$  and  $\text{Al}_2\text{O}_3$  present the best result at 0.3% concentration and productivity increased by 89.42% and 45.19% respectively.  $\text{CuO}$  base SS shows better performance as compared to  $\text{Al}_2\text{O}_3$ ; this is because of high thermal conductivity of  $\text{CuO}$  nanoparticles as compared to  $\text{Al}_2\text{O}_3$ . By increasing the concentration, productivity was increased because increase in the amount of nanoparticles increases the surface area for absorbing solar radiation in the water.

### 3. Previous studies on water depth and tilt angle of condensing cover

Depth of water in the basin of SS and tilt angle of glass cover are the important parameters that affect the SS performance.

It is observed that larger the quantity of water mass inside the basin, the longer it would take to warm up and more energy will be required to heat the basin water. Therefore, if there is a small quantity of water inside the basin, it will heat quickly and require less energy to evaporate.

The latitude based SS gives higher overall year-round productivity as compared to SS with different tilt angles. But if different SS; are designed for different season, then it is found that the SS with lower tilt angle is suitable for summer and SS with higher tilt angle is suitable for winters. Lot of work had been done in past on SS with different water depth and different tilt angle.

The effect of variable water depth from 2 to 12 cm on the performance of plastic-based SS was studied by Phadatar and Verma [30] the highest productivity of 2.1 L/d was found at the lowest water depth (2 cm). Tiwari and Tiwari [4] experimentally investigate the annual and seasonal performance of SS at different water depth. The result found that in both summer and winter season, productivity was higher at lower water depth.

Bataineh and Abbas [31] studied the effect of water depth and wind velocity on the productivity of solar still. They concluded that the productivity of the SS increases as the water depth decreases and wind velocity increases. The higher water mass require higher thermal inertia to heat the basin water and takes more time to reach the maximum point, but at lower water depths, less energy is needed to reach higher water temperature and water tends to evaporate in less time. The wind carry heat energy from the outer surface of glass cover and release it in the atmosphere, thus decreases the glass cover temperature resulting in increased

condensation rate. To achieve maximum productivity in winter and summer seasons Tiwari et al. [32] optimized the inclination of glass cover. Tilt angles of 10°, 30° and 60° for glass cover had been chosen for theoretical study. Based on the tilt angle of the SS, a new convective heat transfer coefficient (HTC) ( $h_m$ ) relation was developed. The authors recommended the lower angle (10°) for the summer season and higher angle for winter season to achieve maximum productivity. Dev and Tiwari [33] conducted an experimental study on 3 different SS having glass covers inclined at 15°, 30°, and 45° and at 4 different water depths (4, 8, 12 and 16 cm). Aljoubouri [34] on the different tilt angle (20°, 31°, 45° and 50°) and differential water depth (1, 2, 3, 5, and 7 cm.).

In both the research it was found that the productivity was higher at the lower angle and lower water depth.

From the literature review, it can be concluded that lower water mass and higher angle gives higher productivity in summer season as lower water mass require less quantity of energy to heat up in a very short period and vice versa for winter season. The inclination angle of the glass cover is one of the important parameters affecting the internal and external heat transfer and water evaporation rate. In summer, the position of the sun is above the latitude; due to which, the solar radiation incident normal at lower angle of SS and maximum quantity of solar insolation

reaches to the basin liner. Whereas in the winter period, the position of the sun is below the latitude, hence SS at higher angle receive as maximum amount of solar radiation; the solar radiation is incident to the normal direction of the glass cover. Therefore, a lower angle of SS for the summer season and higher angle for the winter season is considered as an optimum angle.

An experimental study on passive SS was done by Kumar et al. [35]. They studied the effect on internal heat transfer at three different water depths (5, 10 and 15 cm) and two different tilt angles (30° and 23°). It was concluded that the 30° inclined glass cover provide best performance at 5cm water depth. The experiment was held in the month of March and in this month the sun position is near to the latitude, hence, the incident radiation was normal to the glass cover, which gives higher vaporization rate and higher productivity.

#### 4. Setup description

A schematic diagram and experimental setup of passive single slope SS with three different tilt angles of the condensing cover (11°, 26°, and 41°) and a conventional SS at 26° is shown in Figs. 1a, b and 2. All SSs are fabricated and installed at Solar Lab of M.I.T.S Gwalior Campus

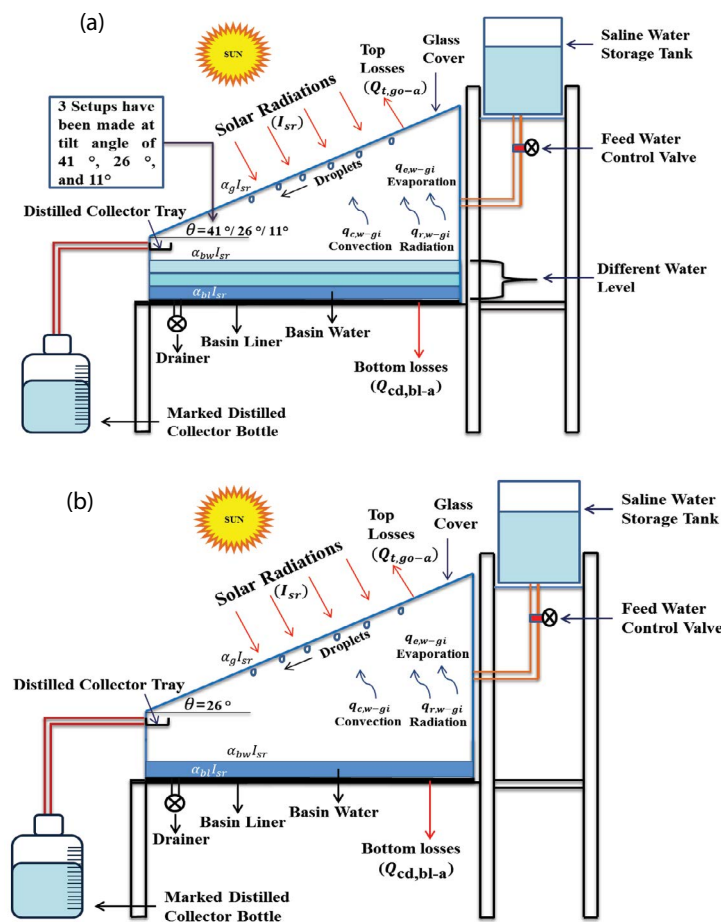


Fig. 1. Schematic diagram of (a) passive SS at different tilt angle of condensing cover and (b) conventional SS.

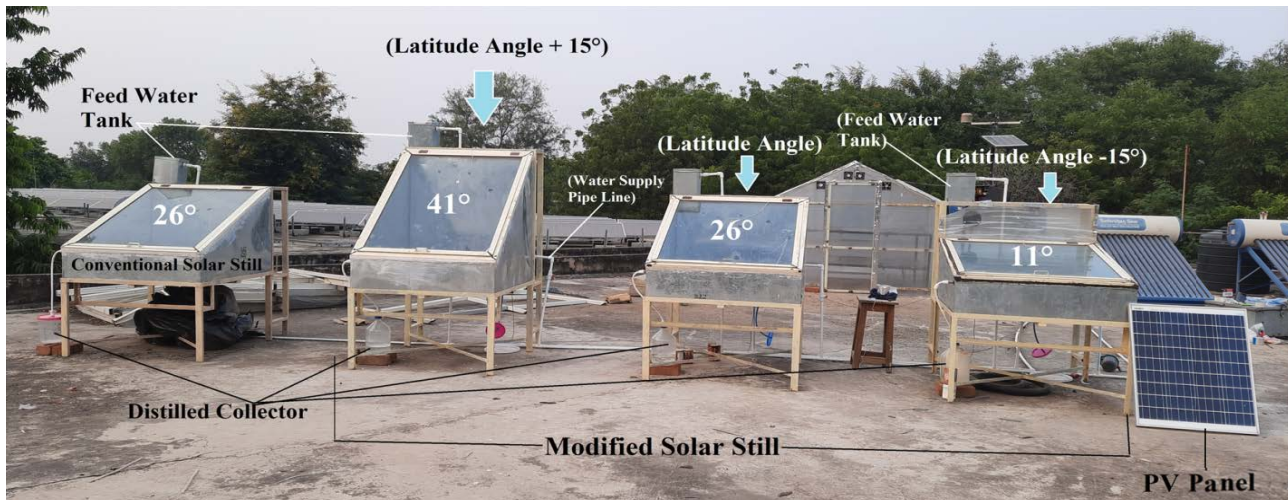


Fig. 2. Experimental setup with different tilt angle of glass cover.

(26.2183° N, 78.1828° E), India. Solar still is made up of 2 cm thick wood and a 2 cm thick layer of thermocol to minimize the heat losses from the bottom and the side walls. The internal and external surface of the solar still is covered with stainless steel sheet. The basin of SS has dimension of 1 m × 1 m and is painted by selective black paint to enhance its absorptivity. Three solar stills are fabricated at different tilt angles. In first still the tilt angle is taken 26° (Latitude of Gwalior), in second still it is kept 11° (Latitude minus 15°) and in third still, it is kept 41° (Latitude plus 15°). The lower height of the still is kept 0.2 m, whereas the higher height of the still is 0.4, 0.7, and 1.07 m and for 11°, 26°, and 41° solar still respectively. A 4 mm toughened glass has been used as the condensing cover of SSS and it is properly sealed with silicone gel to prevent air leakage. To collect the condensate from the glass, a suitable tray is provided inside the still. An aspirator borosilicate bottle has been used to store fresh water coming from the trays of SS. The entire setup is made air tight and leakage proof.

A small water tank of 10 L capacity is provided to compensate the water level in the SS during the experimentation period. Two nanoparticles (CuO and ZnO) are used to enhance the thermal conductivity of the water. For the preparation of nanofluids, a magnetic stirrer and ultrasonic vibrator have been used.

### 5. Instrumentation and uncertainties

An Mastech MS6252A Anemometer is used for measuring the wind velocity, Megger PVM210 Solarimeter was used to measure the radiation falling on inclined glass cover and a (HTC 288-ATH) Hygrometer is used to measure the relative humidity. The temperature of glass cover ( $T_g$ ), basin water ( $T_w$ ), basin liner ( $T_{bl}$ ), vapor ( $T_v$ ), and atmosphere ( $T_a$ ) are measured using digital temperature meter with K-type thermocouples. After every one cycle (24 hr. reading), the basin liner is cleaned to remove scaling and the glass cover is cleaned to remove dust deposited over it. Distilled water was collected in the marked borosilicate aspirator bottle.

There is some uncertainty in the variables measured using various instruments. Based on the accuracy of the various instruments, the standard uncertainty is calculated that shows the possible deviation in measured and calculated parameters. The standard uncertainty is calculated as, [36,37].

$$\text{Standard uncertainty } (\sigma_{un}) = \frac{a}{\sqrt{3}}$$

In the above relation  $\sigma_{un}$  is the standard uncertainty and 'a' is the accuracy of each measuring instrument used during the experiment. The name of equipment's used in the experiment; their range, accuracy, and standard uncertainty is shown in Table 1.

### 6. Methodology

Experiment is carried out in the peak winter season at Solar Energy Lab, MITS, Gwalior (26.2183° N, 78.1828° E), M.P., India. Firstly, three experiments are conducted without nanoparticles at different water depths (4, 5 and 10 cm), after that another experiment are conducted with nanoparticles. A conventional solar still was simultaneously kept operational during experiment on SS with nanoparticles. Experiments were conducted for 9 d in a month to observe the performance of SSS with and without nanoparticles and at 11°, 26°, and 41° tilt angle of glass cover.

In the first three day, all solar still were operated on conventional mode at three different water depths and different tilt angles (11°, 26°, and 41°), in the next set of experiment (3 d) different angles based solar stills were operated with zinc oxide nanoparticles (ZnO) at three different water depths (4, 5 and 10 cm) and on next three days, solar still were operated with copper oxide (CuO) nanoparticles at three different water depth. The constant value used during the computation for all cases is given in Table 2. The period of the experiment per day was 24 h from 7 am to 7 am next morning. The following parameters are measured on hourly basis:

- Wind velocity
- Humidity

Table 1  
Range, accuracy, and % of error for instruments used in experiment

S. No.	Instruments	Type	Range	Accuracy	Standard uncertainty
1.	Temperature indicator with K-type thermocouple	Digital	−50°C–110°C	±1°C	±0.6°C
2.	Solarimeter (Megger PVM210)	Digital	0–1,999 W/m <sup>2</sup>	±5 W/m <sup>2</sup>	±2.886 W/m <sup>2</sup>
3.	Anemometer (Mastech MS6252B)	Digital	0–30 m/s	±0.1 m/s	±0.0577 m/s
4.	Hygrometer (HTC 288-ATH)	Digital	10%–99%	±3%	±1.732%
5.	Aspirator bottle (borosilicate)	Manual	0–5,000 mL	±5 mL	±2.886 mL

Table 2  
Constant value used during the computation for single slope passive solar still [38]

Parameters	Numerical values
$A_g$	1.018, 1.112, and 1.325 m <sup>2</sup> for 11°, 26° and 41°, respectively
$A_b$	1 m <sup>2</sup>
$m_w$	40, 50, and 100 kg for 0.04, 0.05 and 0.1 m water depth, respectively
$\theta$	11°, 26° and 41°
$\alpha_{bl}$	0.30–0.80 (depending upon the condition of still basin)
$\alpha_g$	0.05
$\alpha_w$	0.6
$\epsilon_g$	0.85
$\epsilon_w$	0.95
$L_v$	$2,390 \times 10^3$ J/kg
$d_g$	0.004 m
$K_g$	0.780 W/m°C
$K_{bl}$	0.035 W/m°C
$C_{pw}$	4,184 J/kg°C
$\rho_w$	0.35
$\sigma$	$5.67 \times 10^{-8}$ W/m <sup>2</sup> K <sup>4</sup>
$T$	3,600 s

- Solar radiation till sunset
- Atmospheric temperature
- Outer and inner glass cover, vapor, water and basin liner temperature.
- Distillate output

The flow chart of methodology adopted during the experiment is shown in Fig. 3.

### 6.1. Selection of nanoparticles

In present work, two nanoparticles are used during the experiment. First nanoparticle is copper oxide (CuO), which is having high thermal conductivity (40 W/mK) and other is zinc oxide (ZnO), which is having low thermal conductivity (6.5 W/mK). The specification of both nanoparticles is given in Table 3.

### 6.2. Preparation of nanoparticles

Nanoparticles are hydrophobic in nature; hence it is not soluble in water. If the nanoparticles are directly mixed with water, they settle down within few hours, therefore sonication effect is required. For this, nanofluids are prepared in

two steps. In present experiment, three water depths have been considered; hence the nanofluid is mixed according to maintain the concentrations of nanoparticles at different water depth. First, nanoparticles are weighed on a weighing machine. Then, a magnetic stirrer has been used for 15–20 min to mix nanoparticles and water thoroughly. After that the mixture is placed in a conical flask, and kept in the ultrasonic vibrator machine to make the nanoparticles suspended in water. The sonication effect is provided for almost 45 min to 1 h in the ultrasonic vibrator. Application of this method, does-not allow nanoparticles to settle down in water for at least 12 h.

During the sonication effect, the temperature of the ultrasonic heater coil is kept at 45°C–50°C, which is necessary for an effective sonication. Usually, dispersants are used to keep nanoparticles suspended in water, but in current experimental work it is not used as dispersants increase the boiling point of nanofluids which is not desirable in the case of solar stills. Also, dispersants evaporate with water so the distillate obtained is not potable.

DC stirrer is used inside the SS which is operated for 5 min at an interval of 1 h to keep the nanoparticles suspended in water. Steps involved in preparation of nanofluids are also shown in Fig. 4.

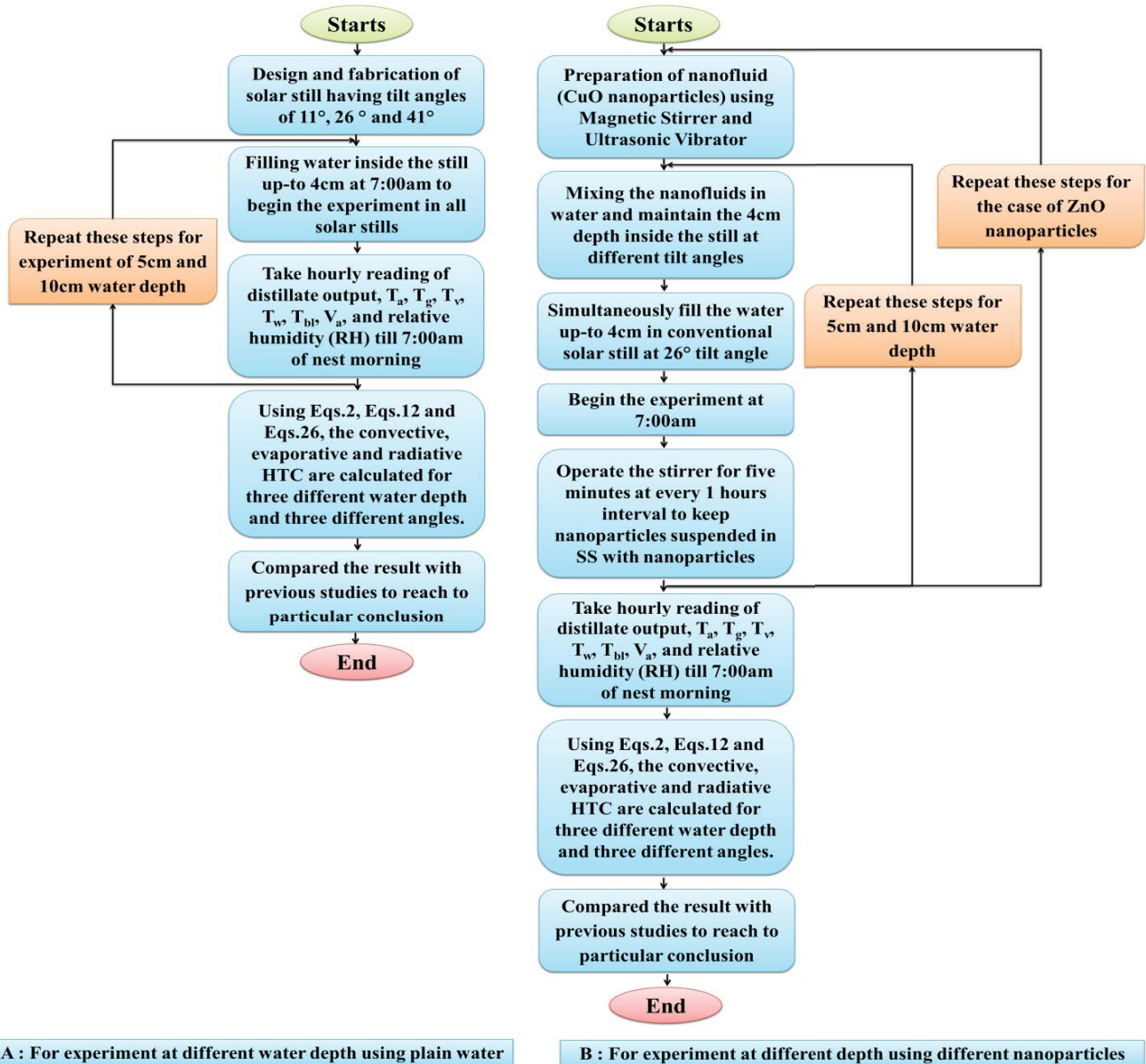


Fig. 3. Flow chart of methodology.

### 6.3. Internal heat transfer analysis

The heat transfer from basin water to the internal glass surface and heat transfer from basin liner to water are considered as internal heat transfer. Internal heat transfer occurs in three ways, radiation, convection and evaporation. The water vapor travels from water to inner glass cover due to buoyancy effect. This process occurs inside the SS due to the temperature difference between the basin water and the glass cover.

The following assumptions have been taken to analyze the heat and mass transfer of various parts of the SS:

- All process in the system are in quasi steady state
- The temperature of the basin fluids is considered uniform throughout its depth.

- The heat capacity of nanoparticles, glass cover and insulated material (sides and bottom) is neglected.
- Setup is air tight and no vapor leakage.

### 6.4. Convective heat transfer

Due to temperature difference of water and glass cover, the rate of the convective heat transfer occurs between the basin water surface and the glass inner surface through water vapor. Temperatures of water ( $T_w$ ) and inner glass surface ( $T_{gi}$ ) are used to find out the convective heat transfer rate inside the still basin. The general equation has been written below to calculate the convective heat transfer inside the SS [39]:

$$Q_{c,w-gi} = h_{c,w-gi} A_w (T_w - T_{gi}) \quad (1)$$

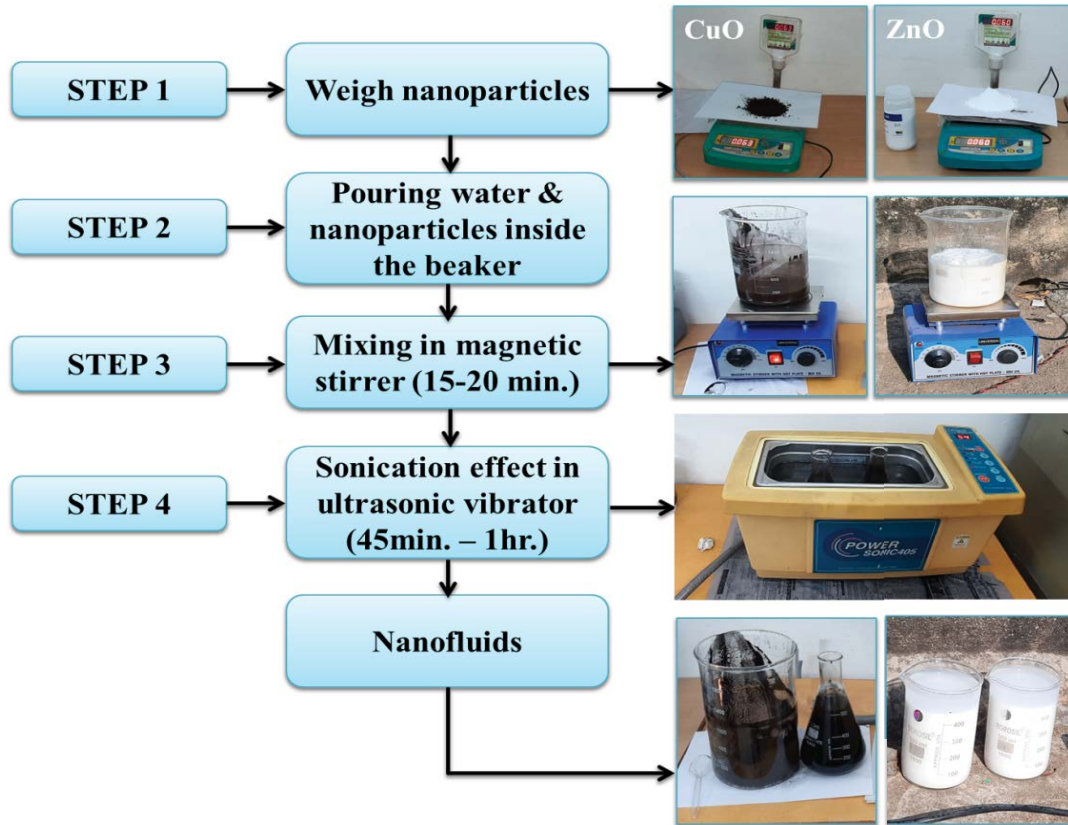


Fig. 4. Steps and equipment’s involve in nanofluids preparation.

Table 3  
Specification of the nanoparticles

Thermophysical properties	Copper oxide	Zinc oxide
Molecular formula	CuO	ZnO
Density (kg/m <sup>3</sup> )	6,400	6,000
Thermal conductivity (W/mK)	40	6.5
Specific heat (J/kg-K)	531	443.4
Average particle size (nm)	30–50	30–50
Appearance	Black	White

where  $h_{c,w-gi}$  is the convective HTC between the water surface and inner surface of the glass cover and it is calculated using the expression given as [40],

$$h_{c,w-gi} = 0.884 \left[ (T_w - T_{gi}) + \frac{(P_w - P_{gi})(T_w + 273)}{(268.9 \times 10^3) - P_w} \right]^{1/3} \quad (2)$$

In 1971, Dunkle [40] first introduced the evaporative and convective heat transfer between the water surfaces and the condensing cover. A drawback of the Dunkle relationship is that the value of  $C$  and  $n$  is fixed for all cases [Eq. (2)]. The value of  $C$  is 0.884 and the value of  $n$  is 1/3. Cooper [42] later expressed the same Dunkle relation with an empirical relation of the Nusselt number, which was

only applicable for normal operation range of SSs. In present work regression analysis is used to find out the value of  $C$  and  $n$  for hourly performance of SS. The following non-dimensional Nusselt number has been used to obtain the convective HTC [43]:

$$Nu = \frac{h_{c,w-gi} L_{cr}}{K_v} = C(Gr \cdot Pr)^n \quad (3)$$

$$h_{c,w-gi} = \frac{K_v}{L_{cr}} \times C(Gr \cdot Pr)^n \quad (4)$$

where  $Gr$  is the Grashof number and  $Pr$  is the Prandtl number, it can be calculated by the following expression:

$$Gr = \frac{\beta_v g L_{cr}^3 \rho_v^2 \Delta T}{\mu_v^2} \quad (5)$$

and

$$Pr = \frac{\mu_v C_{pv}}{K_v} \quad (6)$$

The thermo-physical properties of vapor are calculated by using the expression given in Table 4.

Eq. (4) can also be written as [39]:

$$h_{c,w-gi} = \frac{K_v}{L_{cr}} \times C(R_a)^n \quad (7)$$

Table 4  
Thermophysical properties of water vapor [41]

Properties	Symbol	Expression
Density	$\rho_v$	$353.44/(T_v + 273.15)$
Specific heat	$C_{pv}$	$999.2 + 0.1434 \times (T_v) + 1.101 \times (T_v)^2 - 6.7581 \times 10^{-8} (T_v^3)$
Viscosity	$\mu_v$	$1.718 \times 10^{-5} + 4.620 \times 10^{-8} \times (T_v)$
Thermal conductivity	$K_v$	$0.0244 + 0.7673 \times 10^{-4} \times (T_v)$
Latent heat of vapor	$L_v$	For $T_v > 70^\circ\text{C}$ ; $3.1625 \times 10^6 + [1 - (7.616 \times 10^{-4} \times (T_v))]$ For $T_v < 70^\circ\text{C}$ ; $2.4935 \times 10^6 [1 - (9.4779 \times 10^{-4} \times (T_v) + 1.3132 \times 10^{-7} \times (T_v^2) - 4.7974 \times 10^{-9} \times (T_v^3))]$
Partial pressure at glass cover and water surface	$P$	$P_{gi} = \exp \left[ 25.317 - \left( \frac{5144}{T_{gi} + 273} \right) \right]$ $P_w = \exp \left[ 25.317 - \left( \frac{5144}{T_w + 273} \right) \right]$
Thermal expansion coefficient	$\beta_v$	$1/(T_v + 273.15)$

Ra is the Raleigh number depending on the physical properties of the enclosed air and the temperature difference between water and glass cover. It is calculated as,

$$R_a = \frac{\rho_v g \beta_v L_{cr}^3 \Delta T}{\nu_v \delta_v} = \frac{\rho_v^2 g \beta_v L_{cr}^3 \Delta T}{\mu_v K_v} \quad (8)$$

For a solar still, the value of  $\Delta T$  is calculated as,

$$\Delta T = \left[ T_w - T_{gi} + \frac{(P_w - P_{gi}) T_w}{268.9 \times 10^3 - P_w} \right] \quad (9)$$

The convective HTC ( $h_{c,w-gi}$ ) is dependent on  $C$  and  $n$  which is constant.

The hourly distilled water collection can be determined by the following expression [40]:

$$\dot{m}_{ew} = \left[ \frac{Q_{e,w-gi} \times A_w}{L_v} \right] \times 3,600 \quad (10)$$

where

$$Q_{e,w-gi} = h_{e,w-gi} (T_w - T_{gi}) \quad (11)$$

Malik et al. [44] gave an equation for the evaporation heat loss occurring inside solar stills using mass transfer techniques between the basins water to the condensing surface, which was according to the results of Dunkle [40] and Cooper [42].

### 6.5. Evaporative heat transfer analysis

The evaporative HTC ( $h_{e,w-gi}$ ) can be obtained through the following relation [43]:

$$h_{e,w-gi} = 0.01623 \times h_{c,w-gi} \left( \frac{P_w - RH \times P_{gi}}{T_w - T_{gi}} \right) \quad (12)$$

In Eq. (12), substituting the value of convective HTC ( $h_{c,w-gi}$ ) from Eq. (4), the following relation is obtained:

$$h_{e,w-gi} = 0.01623 \times \frac{K_v}{L_{cr}} \times C (\text{Gr} \cdot \text{Pr})^n \times \left( \frac{P_w - RH \times P_{gi}}{T_w - T_{gi}} \right) \quad (13)$$

Substituting the value of  $h_{e,w-gi}$  in Eq. (11), Eq. (13) becomes [10]

$$Q_{e,w-gi} = 0.01623 \times \frac{K_v}{L_{cr}} \times C (\text{Gr} \cdot \text{Pr})^n \times \left( \frac{P_w - RH \times P_{gi}}{T_w - T_{gi}} \right) \times (T_w - T_{ci}) \quad (14)$$

Or

$$Q_{e,w-gi} = 0.01623 \times \frac{K_v}{L_{cr}} \times C (\text{Gr} \cdot \text{Pr})^n \times (P_w - RH \times P_{gi}) \quad (15)$$

Now, substituting Eq. (15) into Eq. (10), the expression obtained is given as

$$\dot{m}_{ew} = \left[ \frac{0.01623 \times \frac{K_v}{L_{cr}} \times C (\text{Gr} \cdot \text{Pr})^n \times (P_w - RH \times P_{gi}) A_w}{L_v} \right] \times 3,600 \quad (16)$$

The above equation can be simplified as [43]

$$\dot{m}_{ew} = \frac{0.01623}{L_v} \times \frac{K_v}{L_{cr}} \times (P_w - RH \times P_{gi}) A_w \times 3,600 \times C (\text{Gr} \cdot \text{Pr})^n \quad (17)$$

It can be further written as

$$\dot{m}_{ew} = J \times C (\text{Gr} \cdot \text{Pr})^n \quad (18)$$

Or

$$\frac{\dot{m}_{ew}}{J} = C (\text{Gr} \cdot \text{Pr})^n \quad (19)$$

where

$$J = \frac{0.01623}{L_v} \times \frac{K_v}{L_{cr}} \times (P_w - RH \times P_{gi}) A_w \times 3,600 \quad (20)$$

In Eq. (19) taking log on both sides and comparing them with the straight line equation given as [39]

$$y = mx + C \quad (21)$$

Following expressions are found

$$y = \ln\left(\frac{\dot{m}_{ew}}{J}\right), \quad C_1 = \ln C, \quad x = \ln(\text{Gr} \cdot \text{Pr}) \quad \text{and} \quad m = n$$

Now apply the regression analysis for obtaining the value of  $m$  and  $C_1$ . Following expression is used to calculate the value of  $m$  and  $C_1$  [39]

$$m = \frac{N_{\text{ex}}(\sum xy) - (\sum x)(\sum y)}{(N_{\text{ex}})(\sum x^2) - (\sum x)^2} \quad (22)$$

$$C_1 = \frac{(\sum y)(\sum x^2) - (\sum x)(\sum xy)}{(N_{\text{ex}})(\sum x^2) - (\sum x)^2} \quad (23)$$

Based on the experimental data, the values of  $m$  and  $C_1$  can be found from Eqs. (22) and (23), respectively. With the help of  $m$  and  $C_1$ , the values of constants  $C$  and  $n$  can be obtained through the following expression:

$$C = \exp(C_1) \quad (24a)$$

$$n = m \quad (24b)$$

### 6.6. Radiative heat transfer analysis

The radiation heat transfer between basin water surface and inner surface of glass cover is obtained as [45]:

$$Q_{r,w-gi} = h_{r,w-gi} A_w (T_w - T_{gi}) \quad (25)$$

where  $h_{r,w-gi}$  is the coefficient of radiative heat transfer between water and the glass internal surface, which is calculated as [45]:

$$h_{r,w-gi} = \epsilon_{\text{eff}} \sigma \left[ \frac{(T_w + 273)^4 - (T_{gi} + 273)^4}{T_w - T_{gi}} \right] \quad (26)$$

where  $\epsilon_{\text{eff}}$  is the effective emissivity between the water and the glass internal surface which is expressed as:

$$\epsilon_{\text{eff}} = \left[ \frac{1}{\epsilon_w} + \frac{1}{\epsilon_g} - 1 \right]^{-1} \quad (27)$$

Total internal heat transfer [45]:

$$h_{t,w-gi} = h_{c,w-gi} + h_{r,w-gi} + h_{e,w-gi} \quad (28)$$

### 6.7. Heat transfer from basin liner to nanofluid (nanoparticles + water)

$$Q_{c,bl-mf} = h_{c,bl-mf} A_{bl} (T_{bl} - T_{mf}) \quad (29)$$

where  $h_{c,bl-w}$  is the convective HTC from basin liner to basin water [46]

$$h_{c,bl-mf} = 0.54 \frac{K_{mf}}{L_{cr}} (\text{Gr} \cdot \text{Pr})^{0.25} \quad (30)$$

where  $K_{mf}$  is the thermal conductivity of mix fluid. The thermophysical properties of nanofluids and water are given in Tables 5 and 6 respectively.

## 7. Results and discussion

The experiment was conducted in cold weather condition in January 2021, at the Solar Energy Laboratory of the MITS, Gwalior campus, India. Experiments are carried out in all different angle based solar still for three different water depth (4, 5 and 10 cm), for two nanoparticles (CuO and ZnO) and for nine consecutive days. The relative humidity inside the SS is recorded around 88% in the first hour (7:00 am–8:00 am) of the experiment and after 1 h it reaches 100% and remains same until the end of the experiment. This happens because the basin water starts vaporizing after an hour of the experiment and the water vapor mixes with the dry-air present in the cavity area of the SS, due to which the air inside the SS becomes saturated. The wind velocity is also measured for 24 h during each day of the experiment. During the 9 d of experiment periods the average wind velocity is 2.25 m/s.

The variation in incident solar radiation during the nine days of experimentation period is shown in Fig. 5.

All the setups receives maximum amount of radiation at noon 12:00 pm–2:00 pm and then gradually decreases till sunset. The experimental work was conducted in the peak cold season, at that time the sun travels lower from the latitude, due to which the higher angle (41°) is located in the normal direction for the sun. Hence, 41° tilt angle received maximum amount of solar radiation. Lower angle (11° and 26°) receives less amount of solar radiation, because the sun is not in the normal direction to the lower angle SSs, hence the reflection rate is higher at lower angle as compared to the higher angle.

Figs. 6–8 show the temperature of basin water with and without nanoparticles at different level of water depth. It was found that the water temperature decreases as the water depth increases. This is because of high thermal inertia in the higher depth of base fluids. In the winter season, the intensity of solar radiation is low so there is not enough heat to be obtained from the solar radiation, which greatly affects the atmospheric temperature and water temperature. So the basin water takes a long time to reach the maximum temperature ( $T_{\text{max}}$ ). The presence of nanoparticles in water increases the thermal conductivity of the base fluids, which increases the temperature of water and nanoparticles mixture as compared to plain water. Maximum amount of radiation is received over the

Table 5  
Relations used to calculate thermophysical property of nanofluids [27,47]

Properties	Expression
Specific heat	For CuO and water mixture = $15 < d_{np} < 50 \text{ nm}$ ; $0 < \phi_{np} < 4\%$ [23] $C_{p,mf} = 0.8429 \left(1 + \frac{T_{mf}}{50}\right)^{-0.3037} \left(1 + \frac{d_{np}}{50}\right)^{0.4167} \left(1 + \frac{\phi_{np}}{100}\right)^{2.272}$ $C_{p,mf} = \frac{\left(\frac{\phi_{np}}{100}\right) \rho_{np} C_{p,np} + \left(1 - \frac{\phi_{np}}{100}\right) \rho_w C_{p,w}}{\rho_{mf}} \quad [47,48]$
Density	$\rho_{mf} = \left(\frac{\phi_{np}}{100}\right) \rho_{np} + \left(1 - \frac{\phi_{np}}{100}\right) \rho_w \quad [47]$
Thermal conductivity	where $\phi_{np}$ is the weight percentage and can be obtained through following relation $\phi_{np} = \left(\frac{m_{np}}{m_{np} + m_w}\right) \times 100$ <p>where <math>m_{np}</math> is mass of nanoparticles (in gram) add to the basin water and <math>m_w</math> is the mass of basin water (in mL) respectively.</p> <p>For CuO and water mixture = <math>11 &lt; d_{np} &lt; 150 \text{ nm}</math> &lt; <math>\phi_{np} &lt; 10\%</math>; <math>20 &lt; T_{mf} &lt; 70^\circ\text{C}</math> [23]</p> $K_{mf} = K_w \left[ 0.9843 + (0.398) (\phi_{np})^{0.467} \left(\frac{\mu_{mf}}{\mu_w}\right)^{0.0235} \left(\frac{1}{d_{np} \text{ (nm)}}\right)^{0.2246} - (3.951) \left(\frac{\phi_{np}}{T_{mf}}\right) + (34.034) \left(\frac{\phi_{np}^2}{T_{mf}^3}\right) + 32.51 \left(\frac{\phi_{np}}{T_{mf}^2}\right) \right]$ <p>For ZnO and water mixture [49,50]</p> $K_{mf} = K_w \frac{K_{np} + (n_i - 1)K_w - (n_i - 1)\phi_{np}(K_w - K_{np})}{K_{np} + (n_i - 1)K_w + \phi_{np}(K_w - K_{np})}$ <p>where <math>n_i = 3/\psi</math>, <math>n_i</math> = empirical shape factor, <math>\psi</math> = nanoparticles sphericity, <math>\psi = 1</math> all the nanoparticles are uniformly sized, therefore <math>n_i = 3</math></p>
Viscosity	For CuO and water mixture = $11 < d_{np} < 150 \text{ nm}$ ; $0 < \phi_{np} < 10\%$ ; $20 < T_{mf} < 70^\circ\text{C}$ [23] $\mu_{mf} = (2.414 \times 10^{-5}) \times 10^{\left(\frac{247.8}{T_{mf} - 140}\right)}$
Thermal expansion coefficient	For ZnO and water mixture [50] $\mu_{mf} = \mu_w (1 + 2.5\phi_{np})$ $\beta_{mf} = (1 - \phi_{np})\beta_w + \phi_{np}\beta_{np} \quad [51]$ <p>Or</p> $\beta_{mf} = \frac{2}{T_{bl} + T_w}$

Table 6  
Thermophysical properties of basin water [52]

Properties	Symbol	Expression
Density	$\rho_w$	$999.79 + 0.0683 \times T_w - 0.0107 \times T_w^2 + 0.00082 \times T_w^{2.5} - 2.303 \times 10^{-5} \times T_w^3$
Specific heat	$C_{p,w}$	$4.217 - 0.00561 \times T_w + 0.00129 \times T_w^{1.5} - 0.000115 \times T_w^2 + 4.149 \times 10^{-6} \times T_w^{2.5}$
Viscosity	$\mu_w$	$\frac{1}{(557.82 + 19.408 \times T_w + 0.136 \times T_w^2 - 3.116 \times 10^{-4} \times T_w^3)}$
Thermal conductivity	$K_w$	$0.565 + 0.00263 \times T_w - 0.000125 \times T_w^{1.5} - 1.515 \times 10^{-6} \times T_w^2 - 0.000941 \times T_w^{0.5}$

higher angle ( $41^\circ$ ) of SS, resulting in higher water temperature as compared to SSs at an angle of  $26^\circ$  and  $11^\circ$ . The temperature of the basin water reaches a maximum of  $55^\circ\text{C}$  in  $41^\circ$  angle SS with copper oxide nanoparticles (CuO) and at 4 cm of water depth, while the maximum water temperature reach to  $52^\circ\text{C}$  and  $50^\circ\text{C}$  at 5 and 10 cm water depth respectively. During the experiment it has been noted that at higher water depth, more energy is required to heat the water and higher water mass takes long time to heat up, due to which basin water starts to evaporate after 2–3 h as compared to lower water depths. Higher water mass stores higher amount of solar radiation, hence water remains hot for a long time which can be clearly observed in Figs. 7 and 8.

### 7.1. Effect on productivity of solar still

The cumulative distilled water productivity at different tilt angle, for different water depth and for with and without nanoparticles is shown in Fig. 9. It is observed that as the water depth increases and tilt angle decreases, the productivity of the solar still (SS) also decreases. SS with copper oxide nanoparticles (CuO) gives higher productivity as compared to SS with zinc oxide nanoparticles (ZnO) and conventional SS. The yield obtained for all the cases is shown in Table 7.

At 4 cm water depth and at  $41^\circ$  inclination angle, conventional SS, solar still with zinc oxide (ZnO) and copper oxide (CuO) nanoparticles gives maximum of 1,315; 1,590 and 2,025 mL/d distilled output respectively. At same water depth and inclination angle the enhancement in productivity is 53.9% and 20.91% higher than conventional solar still for SS with CuO nanoparticles and ZnO nanoparticles respectively. At 5 cm water depth, with  $41^\circ$  angle, SS with copper oxide achieved 89.5% higher productivity than conventional solar still, while zinc oxide showed an increment of 45.7%. It was observed that at 10 cm water depth productivity increases by 74.7% with copper oxide nanoparticles and 46.6% with zinc oxide nanoparticles.

Solar still with CuO and ZnO nanoparticles at  $11^\circ$  tilt angle having 4 cm water depth gives 1,430 and 1,390 mL

distilled water in a day, at the same time plain water based SS at  $26^\circ$  tilt angle gives 1,270 mL fresh water while conventional SS achieved 1,315 mL in a day at  $41^\circ$  tilt angle. Higher angle, SS received maximum amount of solar radiation which increases the base fluid temperature and the evaporation rate, therefore higher angle is considered as the recommended angle for the winter season. It is observed that solar still operating with nanoparticles at lower angle ( $11^\circ$ ) also gives more productivity than the higher angle ( $26^\circ$ ) conventional SS. Therefore, in winters more productivity can be achieved at the lower angle by using nanoparticles in base fluids of solar still.

It is observed that the SS at higher tilt angle ( $41^\circ$ ) and at lower water depth (4 cm) gives higher productivity in SSs with CuO and ZnO nanoparticles and also in conventional SS without nanoparticles. Due to low water mass, the lower water depth reaches to maximum temperature much faster than the higher water depth, there is high thermal inertia in large water mass (10 and 5 cm) so it takes more time to heat up. The addition of nanoparticles further boost up the productivity but CuO having higher thermal conductivity gives higher productivity than ZnO nanoparticles.

### 7.2. Effect on internal heat transfer coefficient

The hourly variation of evaporative HTC, convective HTC and radiative HTC from basin water to inner glass surface for the different tilt angles and different water mass, having zinc oxide (ZnO) and copper oxide (CuO) nanoparticle is shown in Figs. 10–18. It has been found that the internal HTC varies with water depth and glass cover inclination angle. It can be seen that as the angle of the glass cover increases, the HTC also increases, while with the increase in water mass, the HTC decreases.

In all the cases the evaporation, convection and radiation HTC start increasing from morning 7:00 am and reach to its maximum at 1:00 pm to 3:00 pm and then start decreases till 7:00 am next morning. After 3:00 pm, as the intensity of solar radiation decreases, HTC also decreases. Due to low solar intensity the temperature difference between base fluids and

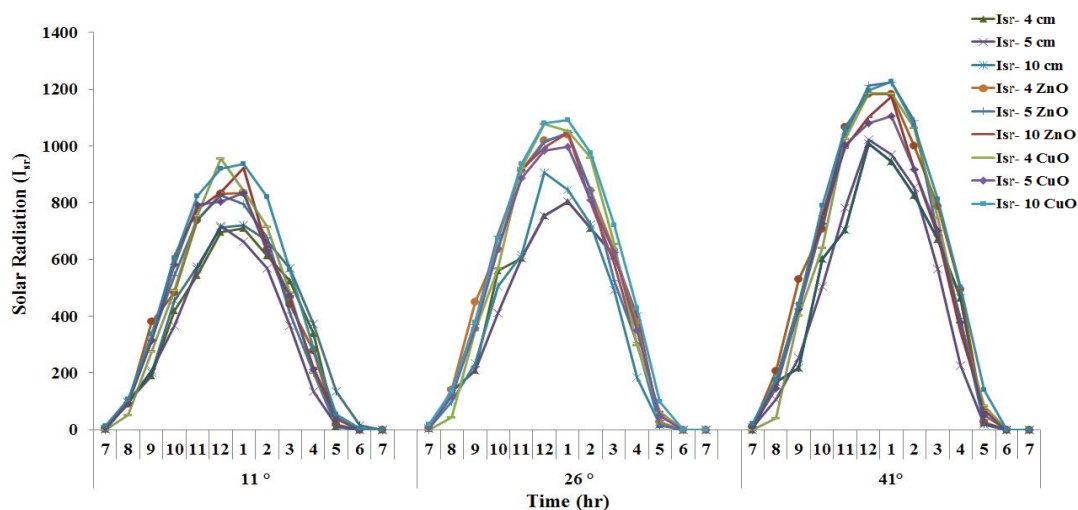


Fig. 5. Solar radiation incident on different angles ( $11^\circ$ ,  $26^\circ$  and  $41^\circ$ ) of solar still (SS), during 9 d experimental period.

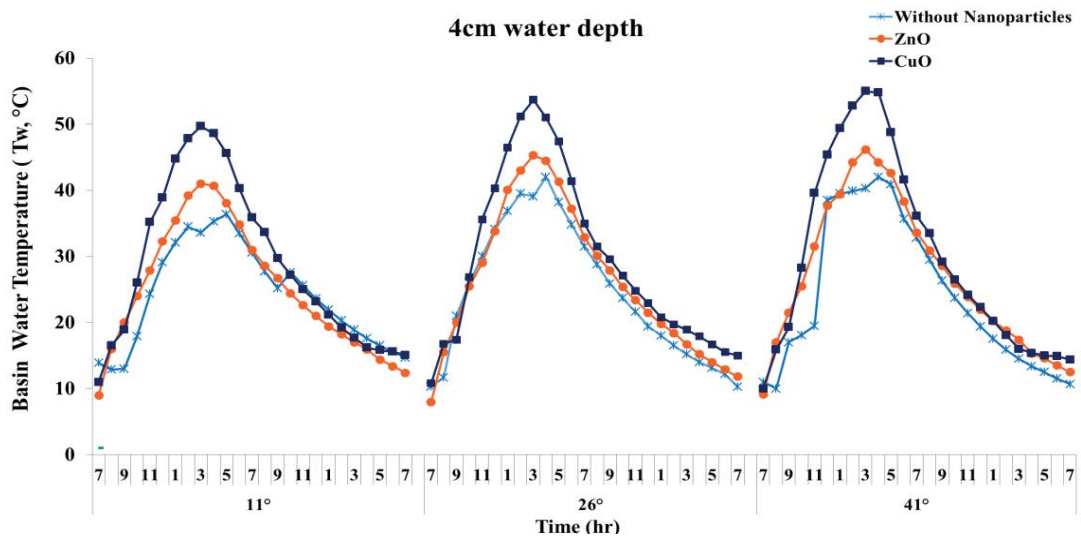


Fig. 6. Hourly variation of basin water temperature with and without nanoparticles for different angle at 4 cm water depth.

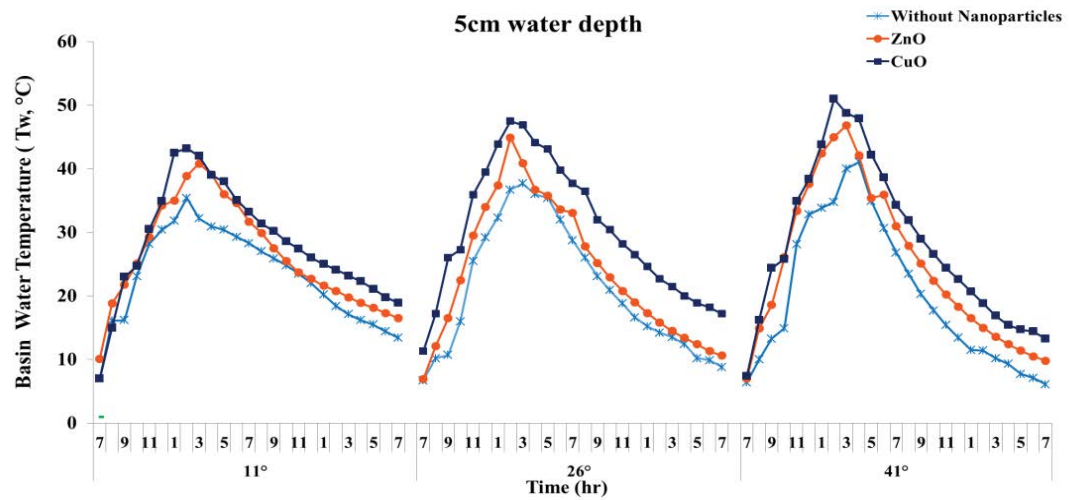


Fig. 7. Hourly variation of basin water temperature with and without nanoparticles for different angle at 5 cm water depth.

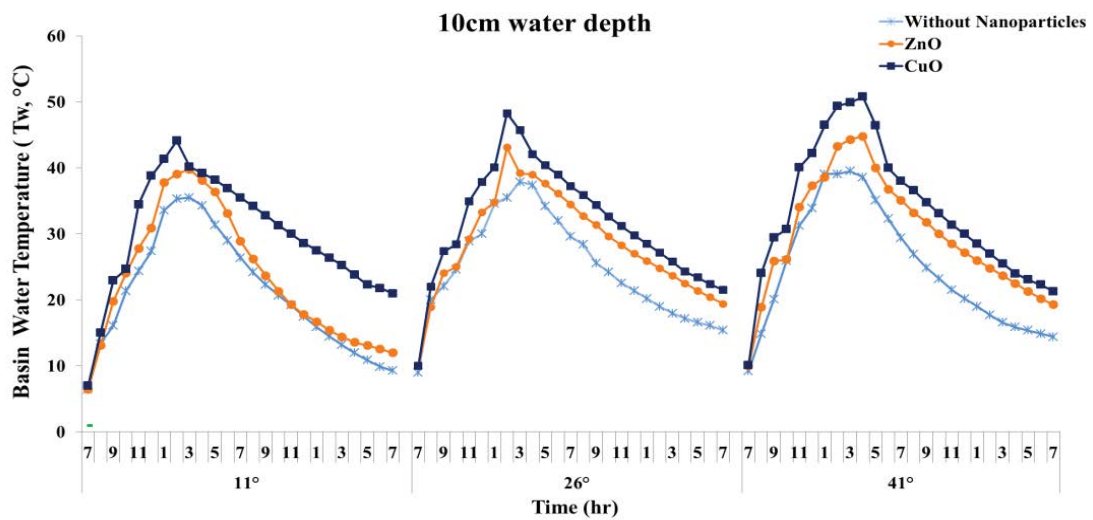


Fig. 8. Hourly variation of basin water temperature with and without nanoparticles for different angle at 10 cm water depth.

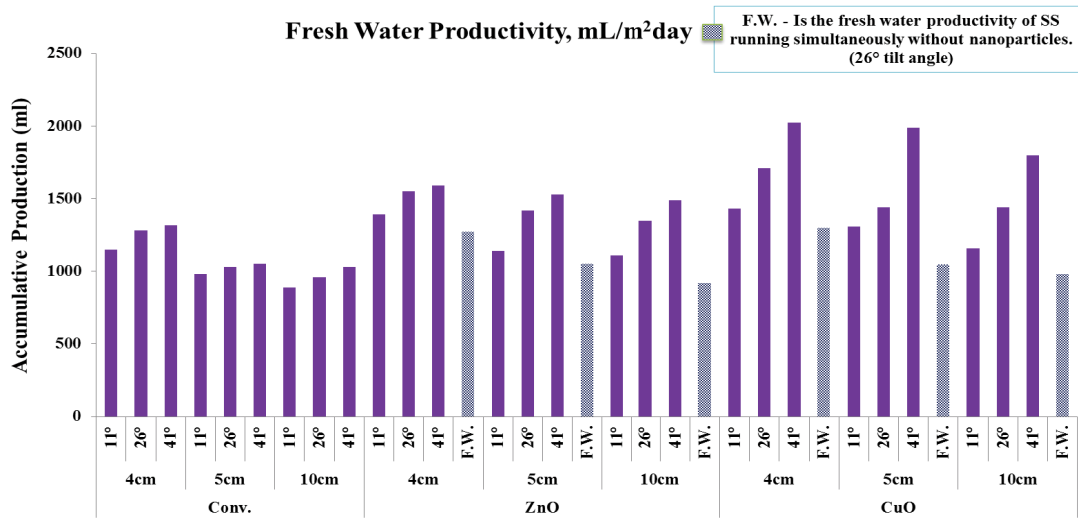


Fig. 9. Daily distilled water productivity for different water depth at different tilt angle, operating with and without nanoparticles.

Table 7  
Accumulative yield of all cases (in mL)

Water depth	Conventional SS			ZnO			F.W.		CuO			F.W.
	11°	26°	41°	11°	26°	41°	26°	11°	26°	41°	26°	
4 cm	1,150	1,280	1,315	1,390	1,550	1,590	1,270	1,430	1,710	2,025	1,300	
5 cm	980	1,030	1,050	1,140	1,420	1,530	1,050	1,310	1,440	1,990	1,045	
10 cm	890	960	1,030	1,110	1,350	1,490	920	1,160	1,440	1,800	980	

glass cover ( $T_w - T_g$ ) gradually decreases, hence the internal HTC starts decreasing after the evening. The partial vapor pressure on the internal glass surface and on the base fluid surface also decreases as it depends on water temperature.

All HTC (evaporation, convection and radiation) is highest at 1:00 pm for all tilt angles (11°, 26° and 41°) with nanoparticles at lower water depth (4 cm), while the time of achieving maximum HTC is shifted to 2:00 pm and 3:00 pm for 5 cm and 10 cm water depth respectively. Due to large water quantity, 10 cm and 5 cm water depth takes more time to heat up; therefore, it takes more time to achieve maximum HTC as compared to lower water depth.

The maximum evaporation HTC is obtained as 72.19 W/m<sup>2</sup>°C, while at 26° tilt angle and at 11° tilt angles it is 38.3688 and 15.919 W/m<sup>2</sup>°C respectively. Zinc oxide based solar still achieved 13.809, 32.6737 and 43.5907 W/m<sup>2</sup>°C maximum evaporation HTC at 11°, 26° and 41° tilt angle of SS at with 4 cm of water thickness, while conventional SS achieved maximum 9.97882, 18.4485 and 23.59 W/m<sup>2</sup>°C evaporative HTC at 4 cm water depth at 11°, 26° and 41° tilt angle of SS. Due to high thermal conductivity copper oxide nanoparticles (CuO) based solar still gives higher internal HTC as compared to zinc oxide (ZnO) and conventional SS. Nanoparticles absorb a large amount of solar radiation and transfer it to the base fluids as a result the convection HTC of the base fluid is increases. A new fact was found that the HTC of nanoparticles-based lower angle SS (11°) was higher than that of without nanoparticles based higher angle of SSs (26°).

The maximum convective and radiative HTC are 3.7036 and 7.08 W/m<sup>2</sup>°C, at higher angle (41°) and lower water depth (4 cm) with copper oxide nanoparticles while, for SS with zinc oxide nanoparticles it is 3.26 and 6.81 W/m<sup>2</sup>°C, and for conventional SS it is 2.34 and 6.53 W/m<sup>2</sup>°C respectively.

Radiative HTC depends upon the water and glass temperature. With increase in water and glass temperature difference ( $\Delta t$ ), the distilled output increases. As the temperature of the glass cover decreases, the water vapors rapidly release their latent heat, which will increase the distilled output.

It is clearly observed that lower water mass (4 cm), high thermal conductive nanoparticles (CuO) and higher angle (41°) based solar still gives better performance as compared to all cases and it was observed that conventional solar still (26° tilt angle) shows better performance compared to lower angle (11° tilt angle) based solar still.

### 7.3. Effect on convective HTC from basin liner to base fluids

The variation in convective HTC from absorber plate (basin liner) to base fluids is shown in Figs. 19–21 for conventional SS, SS with zinc oxide and copper oxide at different water depth (4, 5 and 10 cm) for different tilt angles (11°, 26° and 41°) respectively. It can be seen that nanoparticles-based SS achieved higher convection HTC than the conventional SS. The convective HTC of nanoparticles based still is higher during the maximum sunshine

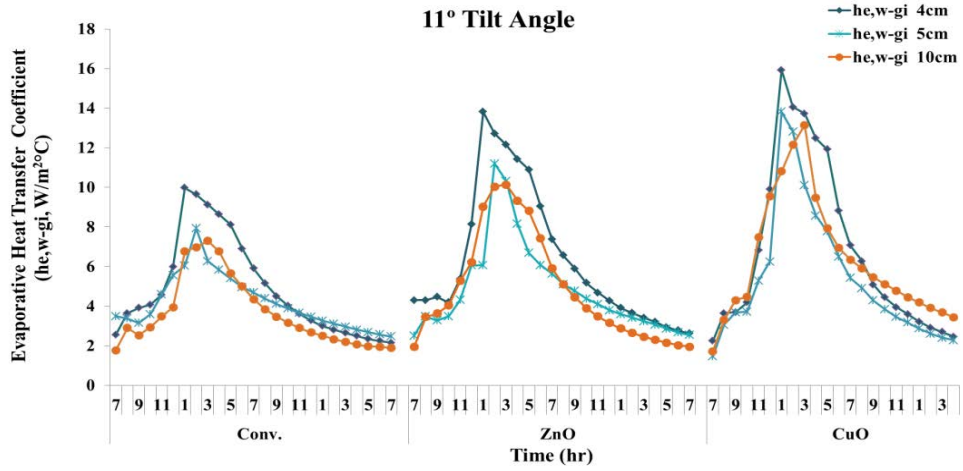


Fig. 10. Hourly variation of evaporative HTC from water to inner surface of glass cover for different water depth (4, 5 and 10 cm) at 11° tilt angle of glass cover.

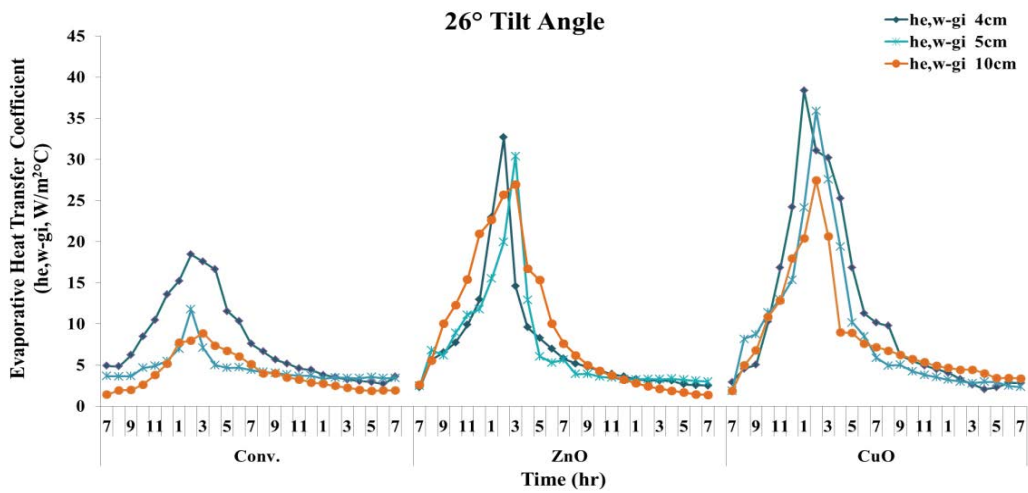


Fig. 11. Hourly variation of evaporative HTC from water to inner surface of glass cover for different water depth (4, 5 and 10 cm) at 26° tilt angle of glass cover.

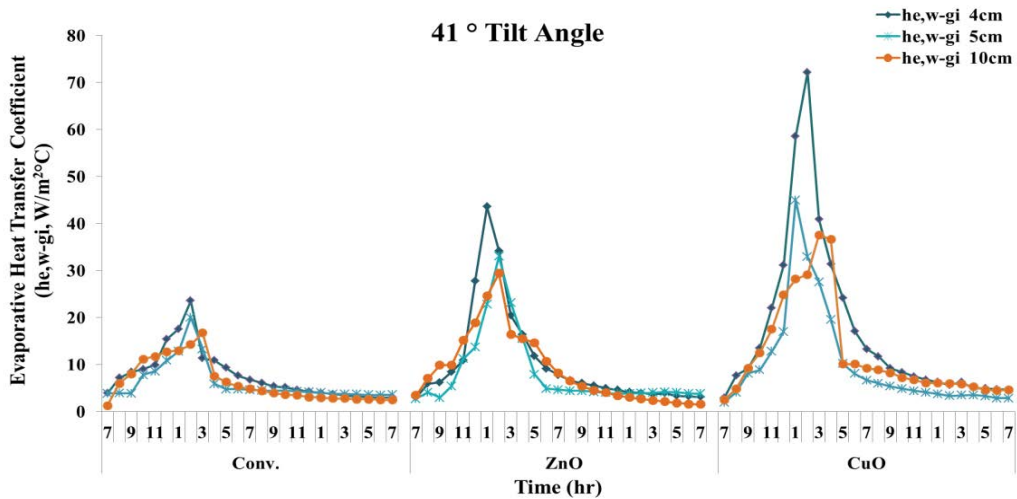


Fig. 12. Hourly variation of evaporative HTC from water to inner surface of glass cover for different water depth (4, 5 and 10 cm) at 41° tilt angle of glass cover.

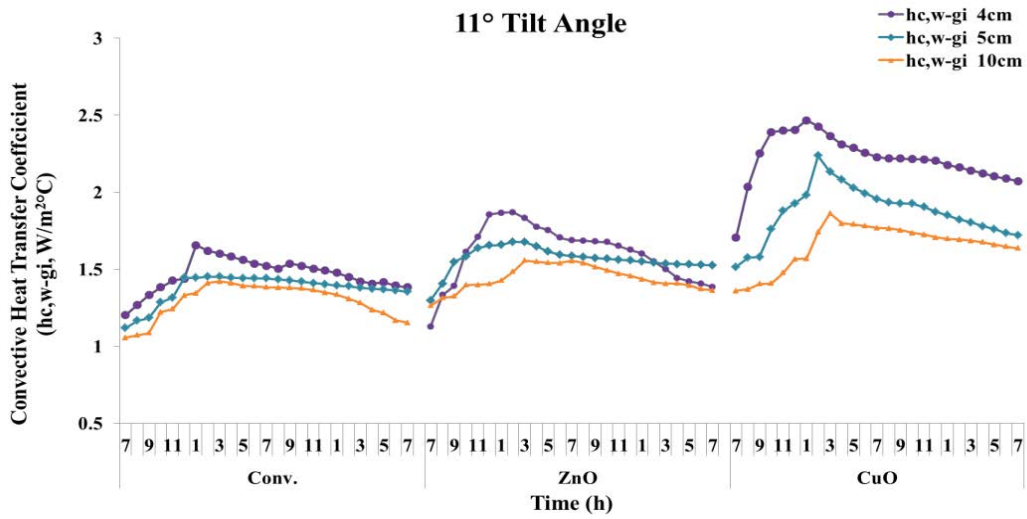


Fig. 13. Hourly variation of convective HTC from water to inner surface of glass cover for different water depth (4, 5 and 10 cm) at 11° tilt angle of glass cover.

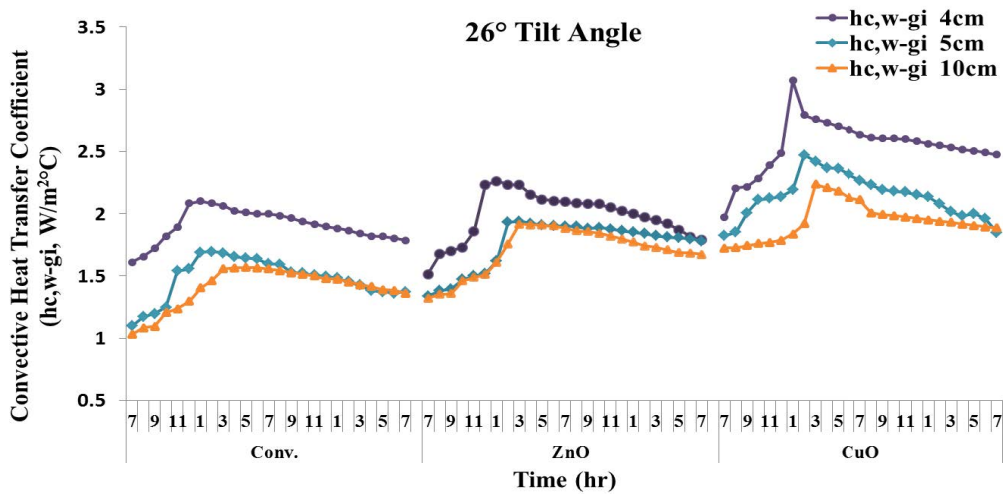


Fig. 14. Hourly variation of convective HTC from water to inner surface of glass cover for different water depth (4, 5 and 10 cm) at 26° tilt angle of glass cover.

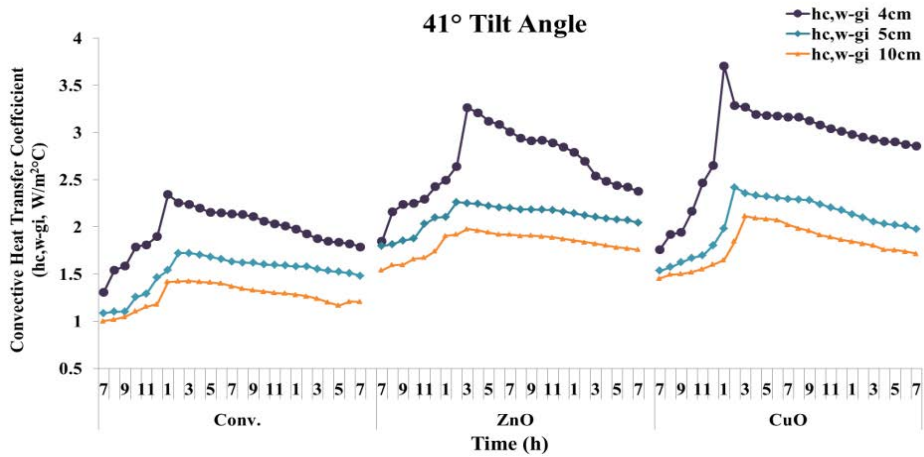


Fig. 15. Hourly variation of convective HTC from water to inner surface of glass cover for different water depth (4, 5 and 10 cm) at 41° tilt angle of glass cover.

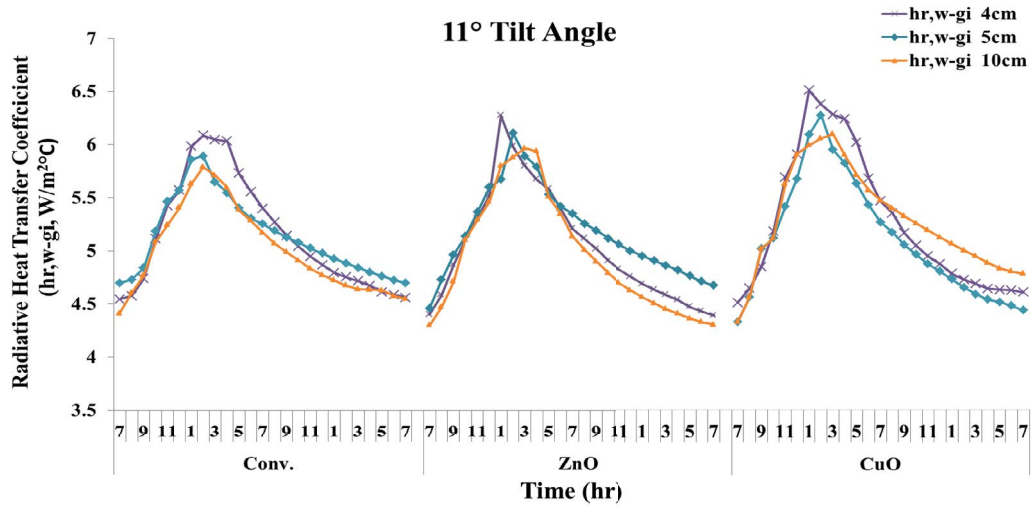


Fig. 16. Hourly variation of radiative HTC from water to inner surface of glass cover for different water depth (4, 5 and 10 cm) at 11° tilt angle of glass cover.

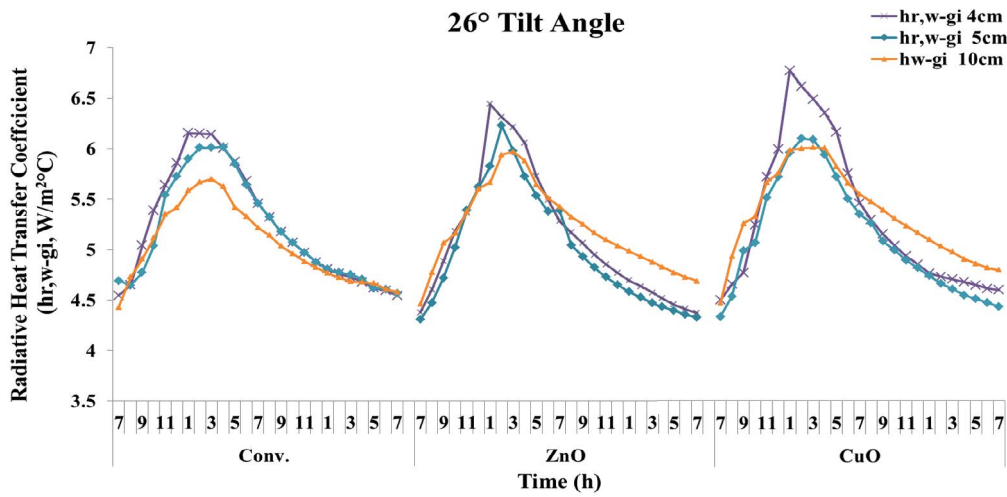


Fig. 17. Hourly variation of radiative HTC from water to inner surface of glass cover for different water depth (4, 5 and 10 cm) at 26° tilt angle of glass cover.

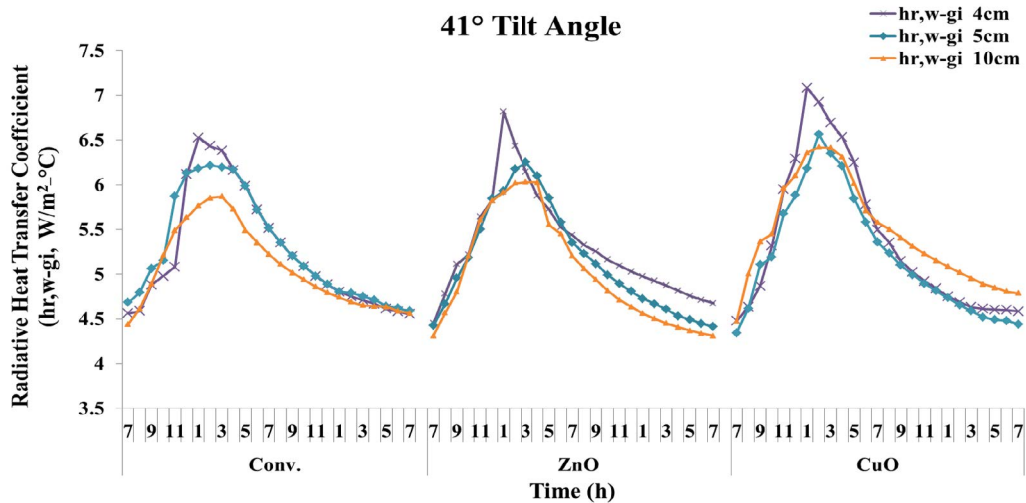


Fig. 18. Hourly variation of radiative HTC from water to inner surface of glass cover for different water depth (4, 5 and 10 cm) at 41° tilt angle of glass cover.

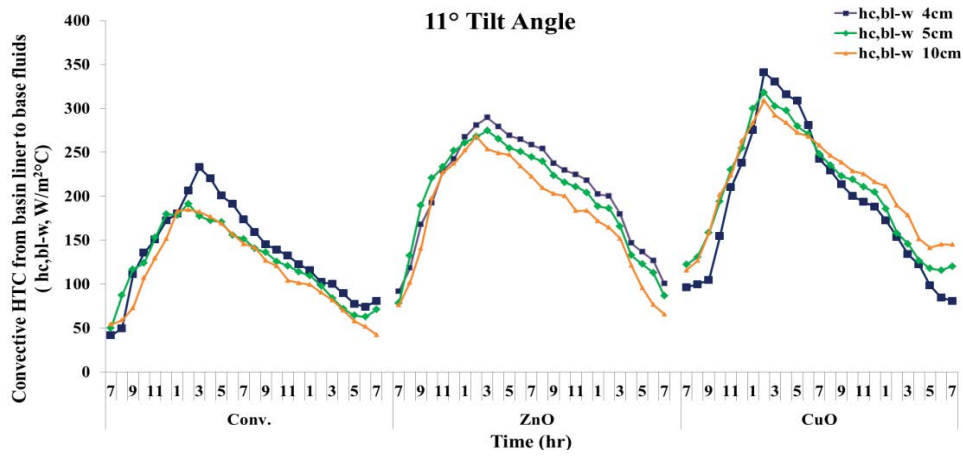


Fig. 19. Hourly variation of convective HTC from basin liner to water and nanofluids at different water depth (4, 5 and 10 cm) and at 11° angle of glass cover.

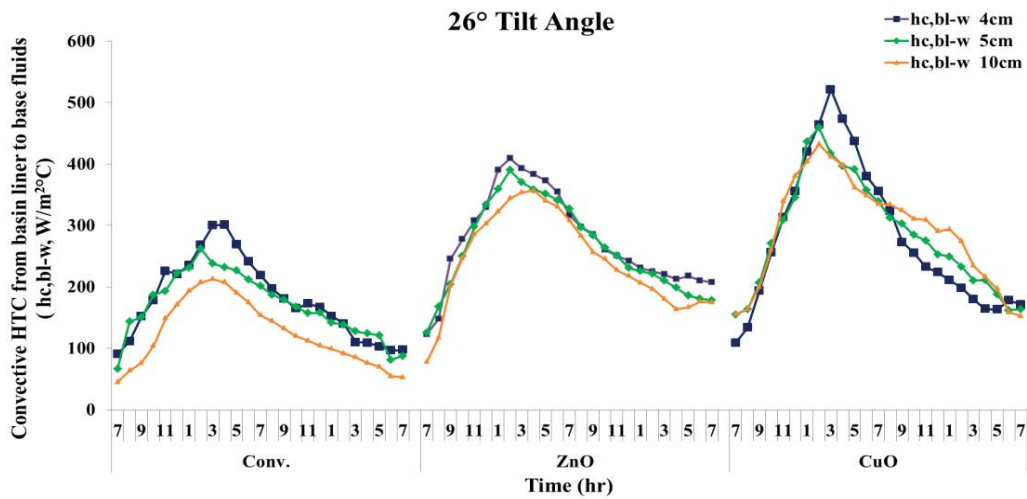


Fig. 20. Hourly variation of convective HTC from basin liner to water and nanofluids at different water depth (4, 5 and 10 cm) and at 26° angle of glass cover.

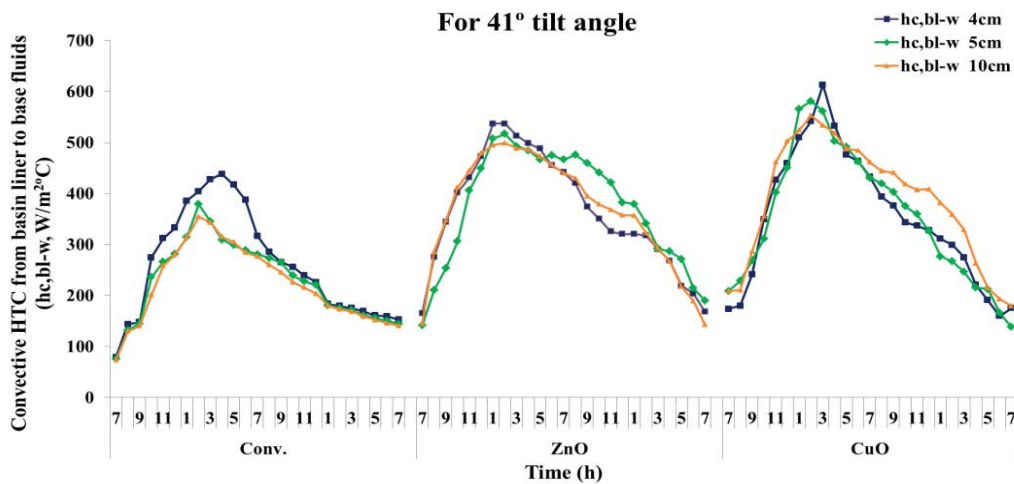


Fig. 21. Hourly variation of convective HTC from basin liner to water and nanofluids at different water depth and at 41° angle of glass cover.

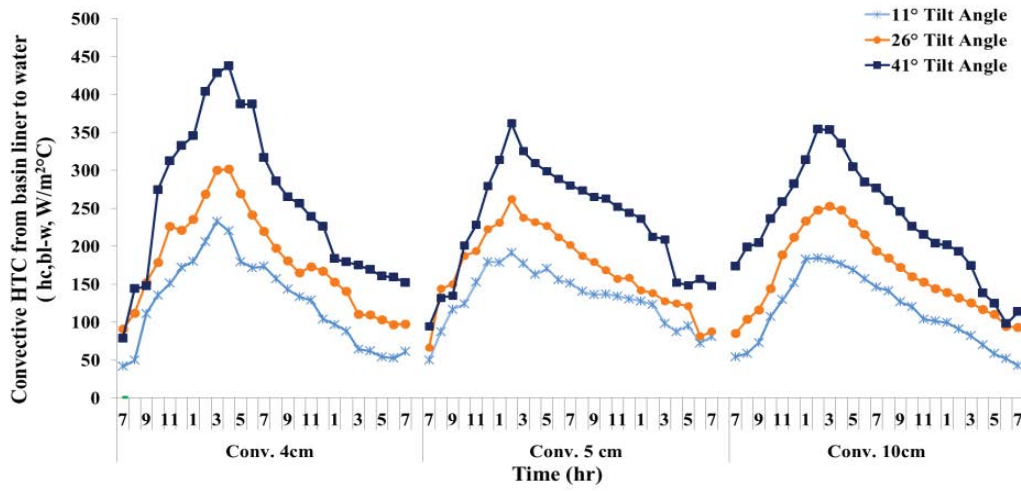


Fig. 22. Hourly variation of convective HTC in conventional solar still from basin liner to water at three different water depth and different tilt angle of glass cover.

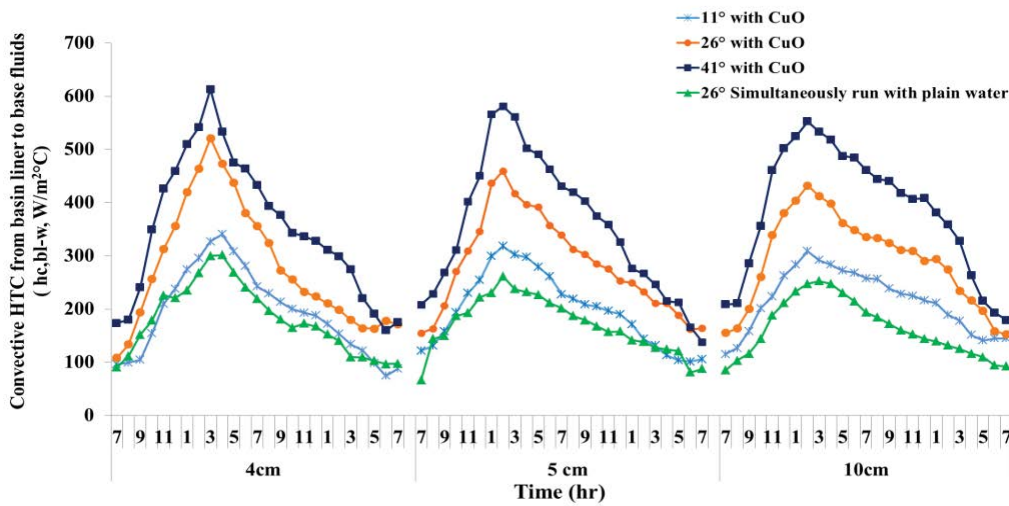


Fig. 23. Hourly variation of convective heat transfer coefficient from basin liner to CuO nanofluids (water + CuO) at three water depth and different tilt angle of glass cover.

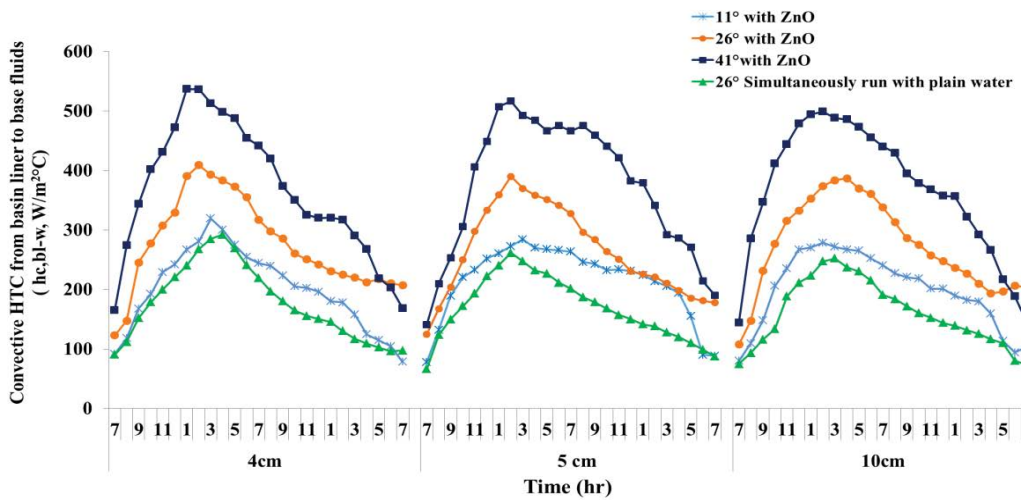


Fig. 24. Hourly variation of convective heat transfer coefficient from basin liner to ZnO nanofluids (water + ZnO) at three water depth and different tilt angle of glass cover.

hours (1:00 pm–2:00 pm), and it is almost 3 times as compared to conventional SS. Presence of nanoparticles is the reason behind these increments. Due to Plasmon resonance absorption band and high thermal conductivity properties, nanoparticles directly absorb the solar radiation and transfer it to the base fluid as thermal energy. Nanoparticles-mixed base fluids have receives two ways of heat energy- first, due to presence of nanoparticles and other from black basin liner. Due to the absence of nanoparticles in conventional solar stills, heat is transferred very slowly from the basin liner.

In Figs. 22–24 it can be seen that there is high convective HTC at lower water depths than other higher water depths, because the low water depth (4 cm) requires less sensible heat as compared to the higher water depth (5 and 10 cm). Fig. 23 shows the first three days performance of solar still without nanoparticles at 4, 5 and 10 cm of water depth. The convective HTC from absorber plate to water increases at the time of 1:00–2:00 pm due to higher radiation received by the setup for all cases. As the intensity of radiation decreases the evaporation rate also decreases. As higher inclination angle receives maximum solar radiation hence the convective HTC is obtained higher. Figs. 24 and 25 show the performance of all three solar stills with copper and zinc, also shows the performance of plain water

based solar still which was running simultaneously during the experimentation. It is observed that plain water based SS gives lower performance as compared to nanoparticles based SS for all cases. A most important thing noticed during the experiment, is that the lower angle, which is not recommended angle for the winter season, gives better performance as compared to higher angle SS without nanoparticles.

It can be clearly seen in Figs. 24 and 25 that lower angle ( $11^\circ$ ) is giving better result as compared to high angle of plain water base conventional SS ( $26^\circ$ ). Therefore, it can be concluded that the nanoparticles loaded lower angle SS can also give better yield in the cold season, it absorbs more amount of heat energy (solar radiation) and rapidly transfer it to basin water, and at the same time heat energy is also obtained from the basin liner.

#### 7.4. Effect on total heat transfer coefficient

The hourly variation of total internal HTC (sum of evaporation, convection, and radiation HTC) from base fluids to inner glass surface at the different tilt angle of the system and at three water depth (4, 5 and 10 cm) is shown in Tables 8–10. It is found that the maximum value of total HTC is achieved between 1:00–2:00pm for lower water

Table 8

The value of total internal HTC at 4 cm water depth for conventional solar still and nanofluids (CuO and ZnO) at three different tilt angles

Time	11° tilt angle			26° tilt angle			41° tilt angle		
	$h_i$ (W/m <sup>2</sup> °C)			$h_i$ (W/m <sup>2</sup> °C)			$h_i$ (W/m <sup>2</sup> °C)		
	Conv.	ZnO	CuO	Conv.	ZnO	CuO	Conv.	ZnO	CuO
7 am	8.29	9.83	8.46	11.06	8.17	9.39	9.78	9.32	9.13
8 am	9.48	10.22	10.33	11.15	11.91	11.39	13.31	12.91	14.26
9 am	9.98	10.73	10.79	12.98	13.10	11.99	14.85	13.58	15.94
10 am	10.57	10.91	11.76	15.70	14.65	17.77	15.79	15.93	21.00
11 am	11.43	12.41	14.91	18.00	17.11	24.93	16.84	18.82	30.45
12 am	13.01	15.51	18.21	21.52	20.78	32.68	23.45	36.00	40.10
1 pm	17.62	21.95	24.89	23.47	31.63	48.21	32.28	53.90	82.40
2 pm	17.35	20.56	22.85	26.68	41.22	40.44	26.44	43.28	69.33
3 pm	16.77	19.77	22.36	25.77	23.03	39.43	19.96	29.84	50.86
4 pm	16.25	18.88	21.03	24.64	17.77	34.34	19.23	25.48	41.04
5 pm	15.41	18.24	20.22	19.43	16.10	25.67	17.43	20.62	33.63
6 pm	14.00	16.14	16.75	18.01	14.59	19.69	15.52	17.73	26.06
7 pm	12.82	14.28	14.76	15.03	13.13	18.23	14.41	16.23	21.97
8 pm	11.94	13.36	13.84	13.93	12.44	17.65	13.57	14.89	20.23
9 pm	11.18	12.59	12.47	12.78	11.89	13.94	12.66	14.23	17.44
10 pm	10.58	11.75	11.70	12.17	11.33	13.16	12.32	13.64	16.45
11 pm	10.06	11.15	11.10	11.48	10.80	12.44	11.63	12.96	15.39
12 pm	9.64	10.65	10.66	11.15	10.40	11.91	11.13	12.49	14.64
1 am	9.27	10.20	10.17	10.49	9.95	11.38	10.74	11.90	13.98
2 am	9.01	9.83	9.80	10.13	9.72	10.53	10.41	11.58	13.30
3 am	8.78	9.49	9.51	9.79	9.63	9.85	10.00	11.12	13.82
4 am	8.57	9.17	9.22	9.54	9.52	9.25	9.77	11.20	12.54
5 am	8.37	8.82	9.12	9.35	8.98	9.44	9.59	10.54	12.45
6 am	8.22	8.60	9.06	9.12	8.77	9.93	9.39	10.35	12.22
7 am	8.10	8.39	8.95	9.92	8.65	9.89	9.35	10.16	12.11

Table 9  
The value of total internal HTC at 5 cm water depth for conventional still and nanofluids (CuO and ZnO) at different tilt angles

Time	11° tilt angle			26° tilt angle			41° tilt angle		
	$h_i$ (W/m <sup>2</sup> °C)			$h_i$ (W/m <sup>2</sup> °C)			$h_i$ (W/m <sup>2</sup> °C)		
	Conv.	ZnO	CuO	Conv.	ZnO	CuO	Conv.	ZnO	CuO
7 am	9.31	8.27	7.29	9.44	8.12	8.02	9.63	8.98	7.80
8 am	9.28	9.61	9.20	9.44	12.64	14.54	9.81	10.58	10.26
9 am	9.17	9.79	10.27	9.60	12.28	15.72	10.03	9.74	14.83
10 am	10.06	10.21	10.59	10.94	15.38	18.55	14.20	12.49	15.74
11 am	11.37	11.31	12.57	11.98	17.99	20.60	15.72	18.74	20.15
12 am	12.57	13.31	13.85	12.76	18.94	23.20	18.45	21.63	24.69
1 pm	13.35	13.40	21.32	14.58	22.94	32.29	20.59	30.90	41.90
2 pm	15.27	18.99	21.89	19.48	28.14	44.46	27.98	41.43	53.18
3 pm	13.37	17.88	18.19	14.76	38.31	36.06	21.22	31.72	36.25
4 pm	12.82	15.59	16.47	12.66	20.56	27.68	13.75	23.90	28.12
5 pm	12.25	13.83	15.43	12.13	13.49	18.25	12.43	15.95	18.35
6 pm	11.70	13.08	13.90	11.97	12.56	16.30	12.15	12.68	15.98
7 pm	11.38	12.58	12.65	11.45	12.94	13.47	11.77	12.17	14.30
8 pm	11.01	11.94	12.01	11.05	10.84	12.40	11.43	11.82	13.52
9 pm	10.66	11.53	11.27	10.77	10.74	12.29	11.32	11.75	12.77
10 pm	10.38	11.06	10.73	10.42	10.29	11.42	11.16	11.39	12.12
11 pm	10.09	10.71	10.22	10.14	10.07	10.87	10.86	11.11	11.49
12 pm	9.84	10.35	9.85	10.07	9.77	10.49	10.62	10.78	11.05
1 am	9.59	10.09	9.45	9.62	9.67	10.09	10.39	10.71	10.60
2 am	9.39	9.85	9.08	9.71	9.67	9.72	10.10	10.68	10.11
3 am	9.18	9.63	8.80	9.61	9.56	9.41	10.06	10.74	10.09
4 am	8.98	9.41	8.59	9.49	9.57	9.47	9.93	10.81	10.05
5 am	8.82	9.16	8.46	9.54	9.39	9.44	9.73	10.64	9.80
6 am	8.66	8.90	8.28	9.37	9.24	8.90	9.65	10.36	9.33
7 am	8.52	8.74	8.11	9.37	9.10	8.61	9.65	10.28	9.25

Table 10  
The value of total internal HTC at 10 cm water depth for conventional still and nanofluids (CuO and ZnO) at different tilt angles

Time	11° tilt angle			26° tilt angle			41° tilt angle		
	Conv.	ZnO	CuO	Conv.	ZnO	CuO	Conv.	ZnO	CuO
7 am	7.23	7.50	7.41	6.87	8.36	8.01	6.72	9.33	8.41
8 am	8.58	9.23	9.23	7.75	11.67	11.62	11.62	13.23	11.30
9 am	8.38	9.67	10.72	7.97	16.44	13.77	13.95	16.27	16.13
10 am	9.25	10.55	11.00	8.95	18.90	17.95	17.46	16.80	19.48
11 am	9.97	11.96	14.58	10.35	22.26	20.27	18.36	22.45	25.04
12 am	10.69	13.08	17.03	11.85	28.07	25.50	19.55	26.44	32.50
1 pm	13.74	16.25	18.36	14.68	29.92	28.22	20.13	32.41	36.17
2 pm	14.17	17.40	19.94	15.11	33.39	35.39	21.55	37.34	37.43
3 pm	14.42	17.66	21.10	16.11	34.84	28.89	24.03	24.47	46.11
4 pm	13.76	16.82	17.16	14.55	24.52	17.20	14.70	23.45	44.99
5 pm	12.44	15.86	15.44	13.73	22.87	16.90	13.16	22.12	18.17
6 pm	11.67	14.30	14.29	12.95	17.47	15.35	12.15	18.07	17.89
7 pm	10.90	12.61	13.59	11.84	14.92	14.84	11.41	15.29	16.85
8 pm	10.30	11.65	13.06	10.67	13.36	14.22	10.86	13.48	16.33
9 pm	9.83	10.87	12.54	10.56	12.10	13.62	10.26	12.21	15.62
10 pm	9.45	10.18	12.10	9.98	11.29	13.01	9.90	11.26	14.47
11 pm	9.09	9.64	11.69	9.63	10.64	12.54	9.63	10.66	13.86
12 pm	8.79	9.22	11.28	9.17	10.04	12.02	9.16	9.93	13.15
1 am	8.56	8.86	10.94	8.93	9.55	11.68	8.99	9.45	12.96
2 am	8.31	8.57	10.61	8.62	9.06	11.40	8.73	9.01	12.83
3 am	8.11	8.31	10.31	8.36	8.74	11.32	8.67	8.67	12.61
4 am	7.93	8.10	10.00	8.09	8.41	10.80	8.45	8.55	11.97
5 am	7.81	7.90	9.73	7.89	8.12	10.15	8.42	8.45	11.23
6 am	7.70	7.72	9.58	7.92	8	10.14	8.32	8.35	11.03
7 am	7.58	7.61	9.47	7.84	7.91	10.06	8.20	8.25	11.13

Table 11  
Comparison of the present work with the previous work on water depth, tilt angle and nanoparticles (ZnO and CuO) used to increase the productivity of SS

Types of SS	Angle/depth/nanoparticles	Setup description	Remark
Single slope passive SS (current work)	11°, 26°, and 41° with 4, 5, and 10 cm water depth	Lower height: 0.20 m; Higher heights: 0.297, 0.44, and 0.635 m for 11°, 26°, and 41° tilt angles respectively; Basin area: 1 m <sup>2</sup> ; Glass thickness: 4 mm; Month: January; Season: winter (India)	Conventional solar still gives maximum 1,315 mL/m <sup>2</sup> distilled water at 41° with 4 cm water depth; Average radiation: 706 W/m <sup>2</sup>
Single slope passive SS with nanoparticles (current work)	11°, 26°, and 41° with 4, 5, and 10 cm water depth; CuO and ZnO: 0.05%; Size: 30 nm	Lower height: 0.20 m; Higher heights: 0.297, 0.44, and 0.635 m for 11°, 26°, and 41° tilt angles respectively; Basin area: 1 m <sup>2</sup> ; Glass thickness: 4 mm; Month: January; Season: winter (India)	Solar still with CuO nanoparticles at 41° tilt with 4 cm water depth angle gives 41.16% higher productivity compared to conventional still; Average radiation: 706 W/m <sup>2</sup>
Single slope passive SS [4]	2, 4, 8, 12 and 18 cm	Basin area: 1 m <sup>2</sup> ; Lower height: 0.25 m; Higher height: 0.83 m; Angle: 30°; Glass thickness: 4 mm; Season: winter (India)	2 cm: 658 mL/d; 4 cm: 695 mL/d; 8 cm: 612 mL/d; 12 cm: 609 mL/d; 18 cm: 479 mL/d; Average radiation: 780 W/m <sup>2</sup>
Single slope passive SS [33]	15°, 30°, and 45° with 4, 8, 12 and 16 cm water depth	Lower height: 0.15 m; Higher heights: 0.42, 0.73, and 1.15 m for 15°, 30°, and 45° tilt angles respectively; Basin area: 1 m <sup>2</sup> ; Glass thickness: 4 mm; Month: November; Season: winter (India)	Maximum yield was achieved at 4 cm water depth; 15°: 812 mL/m <sup>2</sup> /d; 30°: 594 mL/m <sup>2</sup> /d; 45°: 824 mL/m <sup>2</sup> /d; Average radiation: 740 W/m <sup>2</sup>
Single slope passive SS [31]	0.5 to 8 cm water depth	Effective basin area: 1 m <sup>2</sup>	Maximum and minimum productivity achieved on lower and higher water depth respectively; 0.5 cm: 4,211 mL/m <sup>2</sup> /d; 8 cm: 2,620 mL/m <sup>2</sup> /d
Double slope passive SS [53]	TiO <sub>2</sub> , Al <sub>2</sub> O <sub>3</sub> , and CuO: 0.25%; Size: 20 nm	Lower height: 0.22 m; Higher height: 0.534 m; Inclination angles: 30°; Basin area: 2 m <sup>2</sup> × 1 m <sup>2</sup> ; Glass thickness: 4 mm; Month: September; Season: rainy (India)	SS with CuO gives higher productivity compared to conventional still; TiO <sub>2</sub> : 2,710 mL/m <sup>2</sup> ; Al <sub>2</sub> O <sub>3</sub> : 2,750 mL/m <sup>2</sup> ; CuO: 2,890 mL/m <sup>2</sup>
Double slope passive SS [19]	TiO <sub>2</sub> , Al <sub>2</sub> O <sub>3</sub> , and ZnO nanoparticles have been used at 1.0% concentration; Water depth: 1.5 cm	Basin area: 0.58 m <sup>2</sup> ; Height of the basin: 0.35 m; Dimension: 1 m × 0.7 m × 0.35 m; Inclination angles: 32°; Glass thickness: 6.4 mm; Month: September; Season: summer (Mexico)	Combination of nanoparticles gives higher productivity compared to single nanoparticles; TiO <sub>2</sub> : 3,880 mL; TiO <sub>2</sub> + ZnO: 4,720 mL; TiO <sub>2</sub> + Al <sub>2</sub> O <sub>3</sub> : 5,460 mL
Single slope passive SS [54]	CuO: 0.12%; Size: not given; Water depth: 10 and 5 cm	Lower height: 0.21 m; Higher height: 0.634 m; Inclination angles: 23°; Basin area: 1 m <sup>2</sup> ; Glass thickness: 4 mm; month: April; Season: summer (India)	Lower water depth attained maximum productivity. Worked with CuO at 10 and 5 cm water depth, productivity increased by 22.42% and 30.072% compared to conventional still respectively
Single slope passive SS [26]	Al <sub>2</sub> O <sub>3</sub> : 394.7 nm; ZnO: 16 nm; SnO <sub>2</sub> : 114.5 nm; Concentration: 0.1%; Water depth: 1 cm	Lower height: 0.1 m; Higher height: 0.389 m; Inclination angles: 30°; Basin area: 0.25 m <sup>2</sup> ; Glass thickness: 4 mm; Month: March–April; Season: summer (India)	Productivity enhancement compared to conventional still: Al <sub>2</sub> O <sub>3</sub> : 29.95%; ZnO: 18.63%; SnO <sub>2</sub> : 12.67%
Single slope passive SS [15]	Steel plate, zinc plate and copper plate have been used inside the SS	Effective basin area: 1 m <sup>2</sup>	High thermal conductive plate gives maximum productivity: copper plate: 4,510 mL/m <sup>2</sup> ; zinc plate: 3,960 mL/m <sup>2</sup> ; steel plate: 3,350 mL/m <sup>2</sup>

depth (4 cm) and 2:00–3:00 pm for higher water depth (5 and 10 cm). This is because of high thermal inertia in higher mass of base fluids. Hence the higher water depth achieves maximum value of total HTC after 1–2 h as compared to lower water depth. The maximum values of total heat HTCs are obtained as 82.40 W/m<sup>2</sup>°C, at 4cm water depth with CuO and for 41° tilt angle, while with ZnO and conventional still it is 53.90 and 32.28 W/m<sup>2</sup>°C respectively. It is observed that the total HTC increases marginally with increase in inclination angle of glass cover. The totals internal HTC of SS with CuO nanoparticles is obtained higher as compared to ZnO and conventional still. As, explained earlier, this is due to high thermal conductivity of CuO than ZnO and water. The comparison of the current work with the other previous research is shown in Table 11.

## 8. Conclusions

In this paper, the effect on productivity of single slope passive SS with different title angle of glass cover has been studied at three water depths and for two nanoparticles. On the basis of experimentation performed in winter season, the conclusions of the study are as follows:

- The maximum productivity is achieved with CuO nanoparticles at 41° tilt angle and 4 cm water depth.
- At same water depth, the productivity increases with increase in tilt angle while at same tilt angle, the productivity increases with decrease in water depth.
- At 41° tilt angle, the solar still with CuO nanoparticle yield 710, 940 and 770 mL/d more than the still without nanoparticles at 4, 5 and 10 cm water depth respectively.
- At 41° tilt angle, the productivity of solar still with CuO nanoparticles is 27.36%, 30.06% and 20.8% higher than the solar still with ZnO nanoparticles at 4, 5 and 10 cm water depth respectively.
- The productivity of solar still with CuO nanoparticles at 11° tilt angle, is observed 115, 260, and 130 mL/d higher than conventional solar still at 41° tilt angle (recommended for winter season) at 4, 5 and 10 cm water depth respectively.
- The use of nanoparticles increases the value of convective and evaporative heat transfer coefficient and hence increase the productivity of solar still

## Acknowledgement

The authors would like to acknowledge the funding acquired from CRS PROJECT (Project Application ID No. 1-5772916950) sanctioned under “TEQIP-III Collaborative Research Scheme (AICTE-TEQIP-III CRS).

## Symbols

$A$	— Area, m <sup>2</sup>
$A_g$	— Glass area, m <sup>2</sup>
$A_{bl}$	— Basin liner area, m <sup>2</sup>
$A_w$	— Basin water area, m <sup>2</sup>
$C, n$	— Constant
$C_{pw}$	— Specific heat of water, J/kg-K
$C_{pv}$	— Specific heat of vapour, J/kg-K

$C_{p,mf}$	— Specific heat of mixture fluids, J/kg-K
$C_{p,np}$	— Specific heat of nanoparticles, J/kg-K
$d_{np}$	— Size of nanoparticles, nm
$d_g$	— Thickness of glass, mm
$Gr$	— Grashof number
$g$	— Gravity, 9.81 m/s <sup>2</sup>
$h_{c,w-gi}$	— Convective HTC from water to glass, W/m <sup>2</sup> °C
$h_{e,w-gi}$	— Evaporative HTC from water to glass, W/m <sup>2</sup> °C
$h_{r,w-gi}$	— Radiative HTC from water to glass, W/m <sup>2</sup> °C
$h_{t,w-gi}$	— Total HTC from water to glass, W/m <sup>2</sup> °C
$h_{c,bl-gi}$	— Convective HTC from basin liner to mixture fluids, W/m <sup>2</sup> °C
$I_{st}$	— Solar radiation, W/m <sup>2</sup>
$K_v$	— Thermal conductivity of vapor, W/m-K
$K_w$	— Thermal conductivity of water, W/m-K
$K_{mf}$	— Thermal conductivity of mixture fluids, W/m-K
$K_{inl}$	— Thermal conductivity of insulation, W/m-K
$L_{cr}$	— Characteristic length, m
$L_v$	— Latent heat of vapor, J/kg
$L_{inl}$	— Thickness of insulation, mm
$\dot{m}_{ew}$	— Mass of evaporation/distilled output, mL
$m_{np}$	— Mass of nanoparticles, g
$m_w$	— Mass of base fluids, mL
$m_{fw}$	— Mass of feed water, mL
$N_{ex}$	— Number of experimental observation in case of steady state condition
$Nu$	— Nusselt number
$n$	— Constant
$P_w$	— Partial vapor pressure on water, Pa
$P_{gi}$	— Partial vapor pressure on inner glass surface, Pa
$Pr$	— Prandtl number
$Ra$	— Raleigh number
$T_w$	— Basin water temperature, °C
$T_{gi}$	— Inner surface temperature of glass cover, °C
$T_v$	— Vapor temperature, °C
$T_{bl}$	— Basin liner temperature, °C
$T_{mf}$	— Temperature of mixture fluids, water + nanoparticles, °C
$T_{am}$	— Ambient temperature, °C
$T_{bf}$	— Base fluid temperature, water/nanofluids, °C
$T_{sky}$	— Sky temperature, °C
$V_d$	— Wind velocity, m/s
$Q_{c,w-gi}$	— Convective heat transfer from water to glass, W/m <sup>2</sup>
$Q_{e,w-gi}$	— Evaporative heat transfer from water to glass, W/m <sup>2</sup>
$Q_{r,w-gi}$	— Radiative heat transfer from water to glass, W/m <sup>2</sup>
$Q_{c,bl-gi}$	— Convective heat transfer from basin liner to water to mixture fluids, W/m <sup>2</sup>
$Q_{fw}$	— Heat gained from feed water, W/m <sup>2</sup>

## Subscripts

am	— Ambient
bl	— Basin liner
fw	— Feed water
v	— Vapor
g	— Glass
gi	— Inner glass surface
go	— Outer glass surface
inl	— Insulation

$w$	—	Water
mf	—	Nanoparticles and water mixture
$m_w$	—	Mass of water
np	—	Nanoparticles
$t$	—	Total
bf	—	Base fluids, water/nanofluids
$c$	—	Convection
$e$	—	Evaporation
$r$	—	Radiative
cd	—	Conduction

### Greek

$\sigma$	—	Stefan Boltzmann constant, $W/m^2 \cdot k^4$
$\phi_{np}$	—	Nanoparticles concentration, %
$\rho_w$	—	Density of water, $kg/m^3$
$\rho_{mf}$	—	Density of mixture fluids, $kg/m^3$
$\rho_{np}$	—	Density of nanoparticles, $kg/m^3$
$\theta$	—	Angle of glass cover
$\alpha_{bl}$	—	Absorptivity of basin liner
$\alpha_g$	—	Absorptivity of glass
$\alpha_w$	—	Absorptivity of basin water
$\mu_v$	—	Dynamic viscosity of vapor, $Ns/m^2$
$\mu_w$	—	Dynamic viscosity of water, $Ns/m^2$
$\mu_{mf}$	—	Dynamic viscosity of mixture fluids, $Ns/m^2$
$\Delta T$	—	Temperature difference, K
$\nu_v$	—	Kinematic viscosity of vapor, $N/m^2$
$\delta_v$	—	Thermal diffusivity of vapor, $m^2/s$
$\beta$	—	Thermal expansion coefficient, $1/K$
$\epsilon_g$	—	Emissivity of glass
$\epsilon_w$	—	Emissivity of water
$\epsilon_{eff}$	—	Effective emissivity
$\psi$	—	Nanoparticles sphericity

### Abbreviations

HTC	—	Heat transfer coefficient
SS	—	Solar still
RH	—	Relative humidity

### References

- [1] V.K. Dwivedi, G.N. Tiwari, Experimental validation of thermal model of a double slope active solar still under natural circulation mode, *Desalination*, 250 (2010) 49–55.
- [2] P. Prakash, V. Velmurugan, Parameters influencing the productivity of solar stills – a review, *Renewable Sustainable Energy Rev.*, 49 (2015) 585–609.
- [3] A.A. El-Sebaei, Effect of wind speed on active and passive solar stills, *Energy Convers. Manage.*, 45 (2004) 1187–1204.
- [4] A.Kr. Tiwari, G.N. Tiwari, Thermal modeling based on solar fraction and experimental study of the annual and seasonal performance of a single slope passive solar still: the effect of water depths, *Desalination*, 207 (2007) 184–204.
- [5] G.N. Tiwari, H.N. Singh, R. Tripathi, Present status of solar distillation, *Sol. Energy*, 75 (2003) 367–373.
- [6] M.K. Gaur, G.N. Tiwari, B. Energy, S. Kumar, Coefficients for indoor simulation for indoor simulation, *Desal. Water Treat.*, 26 (2011) 201–210.
- [7] F.A. Essa, A.S. Abdullah, Z.M. Omara, Rotating discs solar still: new mechanism of desalination, *J. Cleaner Prod.*, 275 (2020) 123200, doi: 10.1016/j.jclepro.2020.123200.
- [8] Z.M. Omara, A.E. Kabeel, A.S. Abdullah, F.A. Essa, Experimental investigation of corrugated absorber solar still with wick and reflectors, *Desalination*, 381 (2016) 111–116.
- [9] D.B. Singh, G.N. Tiwari, I.M. Al-Helal, V.K. Dwivedi, J.K. Yadav, Effect of energy matrices on life cycle cost analysis of passive solar stills, *Sol. Energy*, 134 (2016) 9–22.
- [10] V.K. Dwivedi, G.N. Tiwari, Thermal modeling and carbon credit earned of a double slope passive solar still, *Desal. Water Treat.*, 13 (2010) 400–410.
- [11] F.A. Essa, M.A. Elaziz, A.H. Elsheikh, An enhanced productivity prediction model of active solar still using artificial neural network and Harris Hawks optimizer, *Appl. Therm. Eng.*, 170 (2020) 115020, doi: 10.1016/j.applthermaleng.2020.115020.
- [12] M.K. Gnanadason, P.S. Kumar, V.H. Wilson, A. Kumaravel, Productivity enhancement of a single basin solar still, *Desal. Water Treat.*, 55 (2015) 1998–2008.
- [13] S. Vaithilingam, G.S. Esakkimuthu, Energy and exergy analysis of single slope passive solar still: an experimental investigation, *Desal. Water Treat.*, 55 (2015) 1433–1444.
- [14] T. Arunkumar, K. Raj, D. Denkenberger, R. Velraj, Heat carrier nanofluids in solar still – a review, *Desal. Water Treat.*, 130 (2018) 1–16.
- [15] M. El Hadi Attia, A.M. Manokar, A.E. Kabeel, Z. Driss, R. Sathyamurthy, W. Al-Kouz, Comparative study of a conventional solar still with different basin materials using exergy analysis, *Desal. Water Treat.*, 224 (2021) 55–64.
- [16] F.A. Essa, Z.M. Omara, A.S. Abdullah, S. Shanmugan, H. Panchal, A.E. Kabeel, R. Sathyamurthy, W.H. Alawee, A.M. Manokar, A.H. Elsheikh, Wall-suspended trays inside stepped distiller with  $Al_2O_3$ /paraffin wax mixture and vapor suction: experimental implementation, *J. Energy Storage*, 32 (2020) 102008, doi: 10.1016/j.est.2020.102008.
- [17] S. Shanmugan, F.A. Essa, Experimental study on single slope single basin solar still using  $TiO_2$  nano layer for natural clean water invention, *J. Energy Storage*, 30 (2020) 101522, doi: 10.1016/j.est.2020.101522.
- [18] A.E. Kabeel, R. Sathyamurthy, A.M. Manokar, S.W. Sharshir, F.A. Essa, A.H. Elshiekh, Experimental study on tubular solar still using Graphene Oxide Nano particles in Phase Change Material (NPCM's) for fresh water production, *J. Energy Storage*, 28 (2020) 101204, doi: 10.1016/j.est.2020.101204.
- [19] F. Carranza, C.D. Villa, J. Aguilar, H.A. Borbón-Nuñez, D. Saucedo, Experimental study on the potential of combining  $TiO_2$ ,  $ZnO$ , and  $Al_2O_3$  nanoparticles to improve the performance of a double-slope solar still equipped with saline water preheating Francisco, *Desal. Water Treat.*, 216 (2021) 14–33.
- [20] A.S. Abdullah, F.A. Essa, Z.M. Omara, Y. Rashid, L. Hadj-Tateb, G.B. Abdelaziz, A.E. Kabeel, C. Engineering, P. Sattam, B. Abdulaziz, S. Arabia, Rotating-drum solar still with enhanced evaporation and condensation techniques: comprehensive study, *Energy Convers. Manage.*, 199 (2019) 112024, doi: 10.1016/j.enconman.2019.112024.
- [21] R.P. Arani, R. Sathyamurthy, A. Chamkha, A.E. Kabeel, M. Deverajan, K. Kamalakannan, M. Balasubramanian, A.M. Manokar, F. Essa, A. Saravanan, Effect of fins and silicon dioxide nanoparticle black paint on the absorber plate for augmenting yield from tubular solar still, *Environ. Sci. Pollut. Res.*, 28 (2021) 35102–35112.
- [22] H. Panchal, H. Nurdiyanto, K.K. Sadasivuni, S.S. Hishan, F.A. Essa, M. Khalid, S. Dharaskar, S. Shanmugan, Experimental investigation on the yield of solar still using manganese oxide nanoparticles coated absorber, *Case Stud. Therm. Eng.*, 25 (2021) 100905, doi: 10.1016/j.csite.2021.100905.
- [23] K. Khanafer, K. Vafai, A critical synthesis of thermophysical characteristics of nanofluids, *Int. J. Heat Mass Transfer*, 54 (2011) 4410–4428.
- [24] M. Chen, Y. He, J. Zhu, Y. Shuai, B. Jiang, Y. Huang, An experimental investigation on sunlight absorption characteristics of silver nanofluids, *Sol. Energy*, 115 (2015) 85–94.
- [25] D.G. Subhedar, K.V. Chauhan, K. Patel, B.M. Ramani, Performance improvement of a conventional single slope single basin passive solar still by integrating with nanofluid-based parabolic trough collector: an experimental study, *Mater. Today: Proc.*, 26 (2020) 1478–1481.

- [26] T. Elango, A. Kannan, K.K. Murugavel, Performance study on single basin single slope solar still with different water nano fluids, *Desalination*, 360 (2015) 45–51.
- [27] S.W. Sharshir, G. Peng, A.H. Elsheikh, E.M.A. Edreis, M.A. Eltawil, T. Abdelhamid, A.E. Kabeel, J. Zang, N. Yang, Energy and exergy analysis of solar stills with micro/nano particles: a comparative study, *Energy Convers. Manage.*, 177 (2018) 363–375.
- [28] L. Sahota, V.S. Gupta, G.N. Tiwari, Analytical study of thermo-physical performance of nanofluid loaded hybrid double slope solar still, *J. Heat Transfer*, 140 (2018) 1–44.
- [29] V.J. Navale, Experimental study of masonic solar still by using nanofluid, *Int. Eng. Res. J.*, 2395–1621 (2016) 984–987.
- [30] M.K. Phadatare, S.K. Verma, Influence of water depth on internal heat and mass transfer in a plastic solar still, *Desalination*, 217 (2007) 267–275.
- [31] K.M. Bataineh, M.A. Abbas, Theoretical and experimental investigations on single slope solar still, *Desal. Water Treat.*, 214 (2021) 338–346.
- [32] G.N. Tiwari, J.M. Thomas, E. Khan, Optimisation of glass cover inclination for maximum yield in a solar still, *Heat Recovery Syst. CHP*, 14 (1994) 447–455.
- [33] R. Dev, G.N. Tiwari, Characteristic equation of a passive solar still, *Desalination*, 245 (2009) 246–265.
- [34] A.A. Aljubouri, Design and manufacturing of single sloped solar still: study the effect of inclination angle and water depth on still performance, *J. Al-Nahrain Univ.*, 20 (2017) 60–70.
- [35] D. Kumar, P. Himanshu, Z. Ahmad, Performance analysis of single slope solar still performance analysis of single slope solar still, *Int. J. Emerging Technol. Adv. Eng.*, 3 (2013) 66–72.
- [36] J. Abolfazli, N. Rahbar, M. Lavvaf, Utilization of thermoelectric cooling in a portable active solar still — an experimental study on winter days, *Desalination*, 269 (2011) 198–205.
- [37] L. Kirkup, B. Frenkel, An introduction to uncertainty in measurement using the GUM (Guide to the expression of uncertainty in measurement), *Accredit. Qual. Assur.*, 12 (2007) 51–52.
- [38] A.E. Kabeel, Z.M. Omara, F.A. Essa, Numerical investigation of modified solar still using nanofluids and external condenser, *J. Taiwan Inst. Chem. Eng.*, 75 (2017) 77–86.
- [39] A.K. Tiwari, G.N. Tiwari, Effect of water depths on heat and mass transfer in a passive solar still: in summer climatic condition, *Desalination*, 195 (2006) 78–94.
- [40] R.V. Dunkle, Solar water distillation: the roof type still and a multiple effect diffusor, *Int. Dev. Heat Transfer*, V (1961) 895–902.
- [41] G.N. Tiwari, *Solar Energy: Fundamentals, Design, Modeling and Applications*, Alpha Science International Ltd., England, Narso Publ. House, 2002.
- [42] P.I. Cooper, The transient analysis of glass covered solar still, *Sol. Energy*, 12 (1969) 313–331.
- [43] S. Kumar, G.N. Tiwari, Estimation of convective mass transfer in solar, *Sol. Energy*, 57 (1996) 459–464.
- [44] M.A.S. Malik, G.N. Tiwari, A. Kumar, M.S. Sodha, *Solar Distillation*, Pergamon Press, Oxford, UK, 1982, pp. 59–71.
- [45] V. Velmurugan, C.K. Deenadayalan, H. Vinod, K. Srithar, Desalination of effluent using fin type solar still, *Energy*, 33 (2008) 1719–1727.
- [46] H. Aghaei Zoori, F. Farshchi Tabrizi, F. Sarhaddi, F. Heshmatnezhad, Comparison between energy and exergy efficiencies in a weir type cascade solar still, *Desalination*, 325 (2013) 113–121.
- [47] B.C. Pak, Y.I. Cho, Hydrodynamic and heat transfer study of dispersed fluids with submicron metallic oxide particles, *Therm. Energy. Exp. Heat Transfer: J. Therm. Energy Gener. Transport Storage Convers.*, 11 (1998) 151–170.
- [48] L. Sahota, S. Arora, H.P. Singh, G. Sahoo, Thermo-physical characteristics of passive double slope solar still loaded with MWCNTs and  $Al_2O_3$ -water based nanofluid, *Mater. Today: Proc.*, (2020) 1–6, doi: 10.1016/j.matpr.2020.01.600.
- [49] R.S. Vajjha, D.K. Das, Experimental determination of thermal conductivity of three nanofluids and development of new correlations, *Int. J. Heat Mass Transfer*, 52 (2009) 4675–4682.
- [50] A.E. Kabeel, Z.M. Omara, F.A. Essa, Theoretical with experimental validation of modified solar still using nanofluids and external condenser, *J. Taiwan Inst. Chem. Eng.*, 75 (2017) 77–86.
- [51] C.J. Ho, M.W. Chen, Z.W. Li, Numerical simulation of natural convection of nanofluid in a square enclosure: Effects due to uncertainties of viscosity and thermal conductivity, *Int. J. Heat Mass Transfer*, 51 (2008) 4506–4516.
- [52] C.O. Popiel, J. Wojtkowiak, Simple formulas for thermophysical properties of liquid water for heat transfer calculations (from 0°C to 150°C), *Heat Transfer Eng.*, 19 (1998) 87–101.
- [53] L. Sahota, G.N. Tiwari, Exergoeconomic and environmental analyses of hybrid double slope solar still loaded with nanofluids, *Energy Convers. Manage.*, 148 (2017) 413–430.
- [54] B. Gupta, P. Shankar, R. Sharma, P. Baredar, Performance enhancement using nano particles in modified passive solar still, *Procedia Technol.*, 25 (2016) 1209–1216.